

Noise-Augmented ℓ_0 Regularization of Tensor Regression with Tucker Decomposition

Tian Yan, Yinan Li, Fang Liu*

Applied and Computational Mathematics and Statistics
University of Notre Dame, Notre Dame, IN 46556, USA

Abstract

Tensor data are multi-dimension arrays. Low-rank decomposition-based regression methods with tensor predictors exploit the structural information in tensor predictors while significantly reducing the number of parameters in tensor regression. We propose a method named NA₀CT² (Noise Augmentation for ℓ_0 regularization on Core Tensor in Tucker decomposition) to regularize the parameters in tensor regression (TR), coupled with Tucker decomposition. We establish theoretically that NA₀CT² achieves exact ℓ_0 regularization on the core tensor from the Tucker decomposition in linear TR and generalized linear TR. To our knowledge, NA₀CT² is the first Tucker decomposition-based regularization method in TR to achieve ℓ_0 in core tensors. NA₀CT² is implemented through an iterative procedure and involves two straightforward steps in each iteration – generating noisy data based on the core tensor from the Tucker decomposition of the updated parameter estimate and running a regular GLM on noise-augmented data on vectorized predictors. We demonstrate the implementation of NA₀CT² and its ℓ_0 regularization effect in both simulation studies and real data applications. The results suggest that NA₀CT² can improve predictions compared to other decomposition-based TR approaches, with or without regularization and it identifies important predictors though not designed for that purpose.

keywords: tensor regression (TR), low-rank decomposition, CP decomposition, Tucker decomposition, vectorization, ℓ_0 regularization, sparsity, noise augmentation, generalized linear model

1 Introduction

Tensor data are D -dimensional arrays in the $\mathbb{R}^{I_1 \times I_2 \times \dots \times I_D}$ space. Many applications, such as medical imaging and recommendation systems, contain tensor data. Vectors are 1D tensors ($D = 1$) and matrices are 2D tensors ($D = 2$). A naïve approach for analyzing tensor data is to vectorize tensors and apply traditional regression models to the vectorized data. Not only do regression models on vectorized data involve a number of parameters in this approach, but

*corresponding author (fang.liu.131@nd.edu)

the structural information contained in the original tensors also is not leveraged during the estimation. To overcome these limitations, tensor regression (TR) models are proposed by applying low-rank decomposition to tensors, including the CANDECOMP/PARAFAC (CP) decomposition (Harshman et al., 1970; Carroll and Chang, 1970) and the Tucker decomposition (Tucker, 1966), that would reduce the number of parameters in regression models (e.g. from tens of millions down to a few hundred (Zhou et al., 2013)) while retaining the spatial structure information in tensor data. Even with low-rank decomposition, the number of parameters (p) in TR may still be large relative to the sample size (n). When $n < p$, regularizations on TR parameters are necessary for the parameter to be identifiable; even if $n > p$, regularizations are often employed to improve the generalization of estimated TR.

Guo et al. (2011) apply CP decomposition in linear TR and regularize parameters with Frobenius norm and group-sparsity norm. Zhou et al. (2013) apply CP decomposition and suggest that commonly used regularizers for generalized linear models (GLMs) can be also applied to TR, such as the bl_2 , l_2 , lasso, elastic net, and SCAD regularizers. Signoretto et al. (2014) extend spectral regularization to TR with convex and differentiable loss functions. Liu et al. (2014) impose Frobenius norm on the difference between a full tensor and its CP decomposition and trace norm on its CP components to achieve relaxed rank regularization and use alternating direction method of multipliers (ADMM) for optimization (Boyd et al., 2011). Wimalawarne et al. (2016) investigate regularization based on overlapped trace norm and (scaled) latent trace norm and employ dual optimization to estimate parameters. Song and Lu (2017) impose both nuclear and l_1 norms in linear TR to achieve a mixture of rank and l_1 regularization. Li et al. (2018) employ Tucker decomposition and regularize the core tensor with common regularizers for GLMs. Raskutti et al. (2019) assume that tensor parameters are located in a low-dimensional subspace and convex and weakly decomposable (a relaxed regularity condition on regularizers to study their oracle properties; see van de Geer (2014) regularizers, and propose a convex optimization framework for multi-dimensional responses. The rank of a low-rank decomposition in TR is often assumed known or pre-specified. If the rank is unknown or not prespecified, the method by He et al. (2018) can be applied that assumes sparsity in each unit-rank tensor in CP decomposition and conducts unit-rank tensor regression iteratively. Ou-Yang et al. (2020) impose sparsity regularization on coefficient tensors directly rather than factor matrices from the CP decomposition of the former, and use ADMM for optimization. Roy and Michailidis (2022) decompose a coefficient tensor into a low tubal rank tensor and a sparse tensor and solve a convex optimization problem using ADMM. Chen et al. (2022) consider the correlation between different slices of a coefficient tensor, and propose latent F-1 norm that set an entire slice of the tensor at zero to promote sparsity. Xu et al. (2022) develop a graph regularizer to incorporate domain knowledge (intra-modal relations) in TR that is encoded in a graph Laplacian matrix and apply the approach to financial data.

Many of the methods mentioned above assume convexity on loss functions. Chen et al. (2019) propose a non-convex projected gradient descent algorithm with error bounds on estimated tensors and show superior performance in both statistical error and run-time in examples. l_0 regularization is also non-convex. To our knowledge, there is little work that

explores the ℓ_0 regularization in TR. ℓ_0 regularization is a desirable regularizer in that it sets zero-valued parameters exactly at zero while providing unbiased estimates for non-zero parameters. On the other hand, ℓ_0 regularization is NP-hard. In the setting of GLMs, approximate ℓ_0 regularizations through continuous functions are often used, such as Wei et al. (2018); Tang et al. (2014); Hyder and Mahata (2009); Liu and Li (2016); Dicker et al. (2013); Lv and Fan (2009); Shi et al. (2018), among others. Some of these methods are examined only when the loss function is least squares and do not offer theoretical guarantees that the approximated ℓ_0 regularizations achieve both accurate variable selection and unbiased estimates for non-zero parameters, and some of them would require the development of new optimization procedures to achieve more efficient computation or more accurate results. To our knowledge, these approximate ℓ_0 regularizers have not been examined in TR with CP or Tucker decompositions.

In this study, we propose to achieve ℓ_0 regularization in TR using the noise-augmented (NA) regularization technique. NA has been used for regularizing the estimation and inferences in GLMs estimation and construction of single and multiple undirected graphs (Li et al., 2021; Li and Liu, 2022). It works by augmenting the original data with noisy samples drawn from Gaussian distributions with adaptive variance terms designed to achieve different types of regularizations such as the ℓ_1 , ℓ_2 , elastic net, SCAD, group lasso, as well as ℓ_0 regularizations among others.

We refer to our method as NA_0CT^2 (*Noise Augmentation for ℓ_0 regularization on Core Tensor in Tucker decomposition*). The core tensor in a Tucker decomposition serves as a central and compressed representation of the interactions among the latent factors extracted along the modes of the original tensor and is central to understanding the relationships between the factors along each mode. To our knowledge, NA_0CT^2 is the first to explore the ℓ_0 regularization on the core tensor with the Tucker decomposition in TR. The achieved sparsity on the core tensor elements through NA_0CT^2 signifies the absence of interaction between specific latent factors and can drastically simplify the interpretation: help identify important variables that matter in the prediction and interpret high-dimensional TR models. In addition, NA_0CT^2 is easy to implement and involves a simple noisy data generation step followed by running regular GLMs (without regularizers) on noise-augmented data iteratively, where one can leverage existing software.

In what follows, we first introduce some basic concepts on tensor decomposition and TR in Section 2. We present the NA_0CT^2 method and an algorithm to implement it in Section 3. We apply NA_0CT^2 to both simulated tensor data and two real tensor datasets in Section 4. The paper concludes in Section 5 with some final remarks on NA_0CT^2 and provides future research directions.

2 Preliminaries

Let x denote a scalar, \mathbf{x} denote a vector, \mathbf{X} denote a matrix, and \mathcal{X} denote a $I_1 \times I_2 \times \cdots \times I_D$ tensor, where D is the dimensionality or the *order* of the tensor, the d -th dimension is known

as the d -mode for $d = 1, \dots, D$, and I_d is the dimension of the d -mode. For example, a typical Magnetic Resonance Imaging (MRI) image is of size $256 \times 256 \times 256$. If expressed as a tensor, it is of order 3 and $I_d = 256$ for $d = 1, 2, 3$. We use $x_{i,j}$ to denote the element (i, j) in matrix \mathbf{X} , and x_i to denote element i in vector \mathbf{x} , and $x_{i_1 i_2 \dots i_D}$ to denote the element in position (i_1, i_2, \dots, i_D) in $\mathcal{X} \in \mathbb{R}^{I_1 \times I_2 \times \dots \times I_D}$.

A tensor can be formulated as an *outer product* of D vectors as in $\mathcal{X} = \mathbf{a}^{(1)} \circ \mathbf{a}^{(2)} \circ \dots \circ \mathbf{a}^{(D)}$, where $\mathbf{a}^{(i)} \in \mathbb{R}^{I_i}$ for $1 \leq i \leq D$; the element $x_{i_1 i_2 \dots i_D}$ in \mathcal{X} is given by $a_{i_1}^{(1)} a_{i_2}^{(2)} \dots a_{i_D}^{(D)}$ for $1 \leq i_d \leq I_d$. The *vectorization* of $\mathcal{X} \in \mathbb{R}^{I_1 \times I_2 \times \dots \times I_D}$ is denoted by $\text{vec}(\mathcal{X})$, and $x_{i_1 i_2 \dots i_D}$ is the $(1 + \sum_{d=1}^D (i_d - 1) \prod_{d'=1}^{d-1} I_{d'})$ -th element of $\text{vec}(\mathcal{X})$ (when $d = 1$, $\prod_{d'=1}^{d-1} I_{d'}$ is replaced by 1). The d -mode *matricization* of $\mathcal{X} \in \mathbb{R}^{I_1 \times I_2 \times \dots \times I_D}$ is denoted as $\mathbf{X}_{(d)} \in \mathbb{R}^{I_d \times (I_1 I_2 \dots I_{d-1} I_{d+1} \dots I_D)}$ and $x_{i_1 i_2 \dots i_D}$ is entry (i_d, j) in matrix $\mathbf{X}_{(d)}$, where $j = 1 + \sum_{k=1, k \neq d}^D (i_k - 1) \prod_{m=1, m \neq d}^{k-1} I_m$ (when $k = 1$, $\prod_{m=1, m \neq d}^{k-1} I_m$ is replaced by 1). The d -mode *product* of tensor $\mathcal{X} \in \mathbb{R}^{I_1 \times I_2 \times \dots \times I_D}$ and matrix $\mathbf{A} \in \mathbb{R}^{J \times I_d}$, denoted by $\mathcal{X} \times_d \mathbf{A} \in \mathbb{R}^{I_1 \times I_2 \times \dots \times I_{d-1} \times J \times I_{d+1} \times \dots \times I_D}$, is given by $(\mathcal{X} \times_d \mathbf{A})_{i_1 i_2 \dots i_{d-1} j i_{d+1} \dots i_D} = \sum_{i_d=1}^{I_d} x_{i_1 i_2 \dots i_D} a_{j i_d}$. The *inner product* of two tensors \mathcal{X} and \mathcal{Y} of the same order D is $\langle \mathcal{X}, \mathcal{Y} \rangle$ that is calculated as $\sum_{i_1=1}^{I_1} \sum_{i_2=1}^{I_2} \dots \sum_{i_D=1}^{I_D} x_{i_1 i_2 \dots i_D} y_{i_1 i_2 \dots i_D}$.

In TR, predictors $\mathcal{X}_i \in \mathbb{R}^{I_1 \times I_2 \times \dots \times I_D}$ are tensors and observations $\mathbf{y} = (y_1, y_2, \dots, y_n)$ on response variable Y are assumed to be independently identically distributed. If Y belongs to exponential family distributions, then TR models can be formulated as follows,

$$p(y_i | \mathcal{X}_i, \mathcal{B}, \phi) = \exp \left\{ \frac{y_i \langle \mathcal{X}_i, \mathcal{B} \rangle - B(\langle \mathcal{X}_i, \mathcal{B} \rangle)}{a(\phi)} + h(y_i, \phi) \right\}, \quad (1)$$

where $\mathcal{B} \in \mathbb{R}^{I_1 \times I_2 \times \dots \times I_D}$ contains unknown parameters and is a tensor of the same order as \mathcal{X} . The most straightforward way to run the model in Eqn (1) with a tensor predictor to vectorize \mathcal{X} and \mathcal{B} and run GLM with or without regularization on the vectorized \mathcal{B} . However, the number of parameters $\prod_{i=d}^D I_d$ in \mathcal{B} is usually large, causing difficulty in both estimation and computation, as well as in the interpretability of the estimated model. In addition, the structural information in \mathcal{X} is lost. To reduce the number of parameters while retaining some structural information in the tensor data, TR can be run with a low-rank decomposition of \mathcal{B} , such as Tucker decomposition or the CP decomposition, instead of a fully-parameterized \mathcal{B} .

A *Tucker decomposition* of tensor $\mathcal{B} \in \mathbb{R}^{I_1 \times I_2 \times \dots \times I_D}$ is defined as

$$\begin{aligned} \mathcal{B} &\approx \mathcal{G} \times_1 \mathbf{U}_1 \times_2 \mathbf{U}_2 \times_3 \dots \times_D \mathbf{U}_D = \llbracket \mathcal{G}; \mathbf{U}_1, \mathbf{U}_2, \dots, \mathbf{U}_D \rrbracket \\ &= \sum_{r_1=1}^{R_1} \sum_{r_2=1}^{R_2} \dots \sum_{r_D=1}^{R_D} g_{r_1 r_2 \dots r_D} \mathbf{u}_1^{r_1} \circ \mathbf{u}_2^{r_2} \circ \dots \circ \mathbf{u}_D^{r_D}, \end{aligned} \quad (2)$$

where $\mathcal{G} \in \mathbb{R}^{R_1 \times R_2 \times \dots \times R_D}$ is the *core tensor* with $R_d \leq I_d$, $\mathbf{U}_d \in \mathbb{R}^{I_d \times R_d}$ is a matrix with orthonormal columns for $d = 1, \dots, D$, and $\mathbf{u}_d^{r_d}$ is the r_d -th column of matrix \mathbf{U}_d for $d = 1, \dots, D$. When $R_d = I_d$, the Tucker decomposition in Eqn (2) is an exact representation of the original tensor and “ \approx ” can be replaced by “ $=$ ”. When $R_d < I_d$, the core tensor is often viewed as a compressed representation of the original tensor. The Tucker decomposition can

be regarded as a form of higher-order principal component analysis; \mathbf{U}_d is the ‘‘principle component’’ (latent factor) extracted along the d -mode and the elements in the core tensor measure presents of the interactions among the latent factors.

An rank- R CP decomposition of \mathcal{B} is

$$\mathcal{B} \approx \llbracket \mathbf{g}; \mathbf{U}_1, \mathbf{U}_2, \dots, \mathbf{U}_D \rrbracket = \sum_{r=1}^R g_r \mathbf{u}_1^r \circ \mathbf{u}_2^r \circ \dots \circ \mathbf{u}_D^r, \quad (3)$$

where $\mathbf{g} = (g_1, \dots, g_R) \in \mathbb{R}^R$, $\mathbf{U}_d \in \mathbb{R}^{I_d \times R}$ for $d = 1, \dots, D$, $\|\mathbf{u}_d^r\|_2 = 1$, and is the r -th column of matrix \mathbf{U}_d , and $\mathbf{u}_d^r \in \mathbb{R}^{I_d}$ for $d = 1, \dots, D$. In other words, \mathcal{B} is the sum of R rank-one tensors of dimensions I_1, \dots, I_D , respectively. If \mathcal{B} can be expressed exactly as the sum of R rank-one tensors, then \mathcal{B} admits a rank R decomposition and ‘‘ \approx ’’ in Eqn (3) can be replaced by ‘‘=’’. The CP decomposition can be regarded as a special case of the Tucker decomposition when the core tensor is super-diagonal and R_d in is the same for all $d = 1, \dots, D$ Eqn (2). If we relax the requirement of $\|\mathbf{u}_d^r\|_2 = 1$, g_r in Eqn (3) can be incorporated in any of the \mathbf{u}_d^r terms for $d = 1, \dots, D$. For example, if g_r is multiplied with \mathbf{u}_1 , the CP decomposition can be written as $\sum_{r=1}^R \mathbf{u}'_1 \circ \mathbf{u}_2^r \circ \dots \circ \mathbf{u}_D^r$, where $\mathbf{u}'_1 = \mathbf{g}_r \cdot \mathbf{u}_d^r$ (element-wise multiplication).

Applying the Tucker and CP compositions, $\langle \mathcal{X}_i, \mathcal{B} \rangle$ in the TR model in Eq (2) can be written, respectively, as

$$\langle \mathcal{X}_i, \mathcal{B} \rangle = \langle \mathcal{X}_i, \llbracket \mathcal{G}; \mathbf{U}_1, \mathbf{U}_2, \dots, \mathbf{U}_D \rrbracket \rangle = \langle \mathcal{X}_i, \sum_{r_1=1}^{R_1} \sum_{r_2=1}^{R_2} \dots \sum_{r_D=1}^{R_D} g_{r_1 r_2 \dots r_D} \mathbf{u}_1^{r_1} \circ \mathbf{u}_2^{r_2} \circ \dots \circ \mathbf{u}_D^{r_D} \rangle, \quad (4)$$

$$\langle \mathcal{X}_i, \mathcal{B} \rangle = \langle \mathcal{X}_i, \llbracket \mathbf{g}; \mathbf{U}_1, \mathbf{U}_2, \dots, \mathbf{U}_D \rrbracket \rangle = \langle \mathcal{X}_i, \sum_{r=1}^R g_r \mathbf{u}_1^r \circ \mathbf{u}_2^r \circ \dots \circ \mathbf{u}_D^r \rangle. \quad (5)$$

$\mathcal{G}, \mathbf{g}, \mathbf{u}'$ will thus be estimated instead of the elements in the original tensor \mathcal{B} . As mentioned above, the model based on either of the two decompositions can lead to a potentially significant decrease in the number of parameters while honoring at least partially the structural information in \mathcal{B} compared to a GLM with vectorized \mathcal{B} and \mathcal{X} . Table 1 lists the numbers of free parameters in the original tensor \mathcal{B} , its Tucker decomposition, and its CP decomposition. For CP decomposition, the number of free parameters, compared to that in the original \mathcal{B} , would be much smaller. For example, For $D = 3$ and $I_d = 64$, then the number of parameters goes from 262,144 down to 6,080 if $R = 32$ (97.7% decrease) and down to 12,160 if $R = 64$ (95.3% decrease). In the case of Tucker decomposition, R_d needs to be smaller than I_d at least for some d in order for the number of free parameters to decrease from that in the original \mathcal{B} ; otherwise, the number of parameters would not be reduced though it still has the benefit of honoring the structural information in \mathcal{X} via the decomposition and provides more control over the what parameters to regularize in the model.

Table 1: Number of free parameters in Tucker decomposition and CP decomposition of tensor $\mathcal{B} \in \mathbb{R}^{I_1 \times I_2 \times \dots \times I_D}$ (Li et al., 2018)

	rank- R CP	Tucker	original
$D = 2$	$R(I_1 + I_2) - R^2$	$I_1 R_1 + I_2 R_2 + R_1 R_2 - R_1^2 - R_2^2$	$\prod_{d=1}^D I_d$
$D > 2$	$R(\sum_{d=1}^D I_d - D + 1)$	$\sum_{d=1}^D I_d R_d + \prod_{d=1}^D R_d - \sum_{d=1}^D R_d^2$	

3 Method

Though CP decomposition is simple, it is often limited in its approximation capability and requires \mathbf{u}_d^r to have the same dimension for any fixed d and different r , where $r = 1, 2, \dots, R$ in 3. In Comparison, Tucker decomposition is more flexible and allows different numbers of components in different modes after the decomposition and as well as less structure on the core tensor (CP is a special case of Tucker with a super-diagonal structure for the core tensor). For this reason, we focus on TR decomposition. Interested readers may also refer to (Li et al., 2018) for the comparison between Tucker and CP decompositions when used in the TR setting.

We examine the case when response variable Y follows an exponential family distribution given in Eq (1). The loss function is the negative log-likelihood function of \mathcal{B} (other loss functions without making distributional assumptions, such as the simply ℓ_2 loss or cross-entropy loss, can be used as seen appropriate),

$$l = l(\mathcal{B}|\mathbf{y}, \mathcal{X}_i, 1 \leq i \leq n) = - \sum_{i=1}^n \ln p(y_i|\mathcal{X}_i, \mathcal{B}). \quad (6)$$

Our proposed method NA₀CT² applies Tucker decomposition to \mathcal{B} (Eq (2)) and uses an iterative procedure to estimate the core tensor \mathcal{G} with ℓ_0 regularization and \mathbf{U}_d for $d = 1, \dots, D$. Since the core tensor represents the interaction among the factor matrices in the Tucker decomposition of \mathcal{B} , it being sparse implies that there are only limited interactions among the factor matrices, which helps with interpretations.

Each iteration t in the NA₀CT² algorithm contains two simple steps: 1) generate noisy data $(\mathcal{Z}_j^{(t)}, e_{y,j}^{(t)})$ for $j = 1, \dots, n_e$ given the updated tensor estimate from iteration $t - 1$; 2) run GLM on the updated noise-augmented data

$$\begin{bmatrix} (\mathcal{X}_i, y_i)_{i=1, \dots, n} \\ (\mathcal{Z}_j^{(t)}, e_{y,j}^{(t)})_{j=1, \dots, n_e} \end{bmatrix}. \quad (7)$$

Values of noisy response data $e_{y,j}^{(t)}$ depend on the type of TR. For linear TR, we may set $e_{y,j}^{(t)} \equiv 0$, the sample mean \bar{y} , or any other constant d for $j = 1, \dots, n_e$; for logistic TR with $Y = \{0, 1\}$, we may set half of n_e $e_{y,j}^{(t)}$'s at 0 and the other half at 1; for Poisson and negative binomial TR, we may set $e_{y,j}^{(t)} = 1$ for $j = 1, \dots, n_e$. Augmented tensor predictor $\mathcal{Z}_j^{(t)}$ is constructed from the components of a Tucker decomposition; that is,

$$\begin{aligned} \mathcal{Z}_j^{(t)} &\triangleq \mathcal{E}_j^{(t)} \times_1 \mathbf{U}_1^{(t-1)} \times_2 \mathbf{U}_2^{(t-1)} \times_3 \cdots \times_D \mathbf{U}_D^{(t-1)} \\ &= \sum_{r_1=1}^{R_1} \sum_{r_2=1}^{R_2} \cdots \sum_{r_D=1}^{R_D} e_{j, i_1 i_2 \dots i_D}^{(t)} \mathbf{u}_1^{r_1(t-1)} \circ \mathbf{u}_2^{r_2(t-1)} \circ \cdots \circ \mathbf{u}_D^{r_D(t-1)}, \end{aligned} \quad (8)$$

$$\text{where } e_{j, i_1 i_2 \dots i_D}^{(t)} \sim \mathcal{N}(0, \lambda (g_{r_1 r_2 \dots r_D}^{(t-1)})^{-2}), \quad (9)$$

λ is a hyperparameter (tuned or prespecified), $g_{r_1 r_2 \dots r_D}^{(t-1)}$ is the element $[r_1, r_2, \dots, r_D]$ in the core tensor $\mathcal{G}^{(t-1)}$, and $\mathbf{U}_i^{(t-1)}$ for $i = 1, \dots, D$ is the estimate of \mathbf{U}_i from iteration $t - 1$; both

$\mathcal{G}^{(t-1)}$ and $\mathbf{U}_i^{(t-1)}$ are the components in the Tucker decomposition of estimate $\mathcal{B}^{(t-1)}$. Eq (9) is referred to as the *noise-generating distribution*, a Gaussian distribution with an adaptive variance term that is designed to achieve ℓ_0 regularization. In addition, n_e needs to be $< p$, where p is the total number of elements in \mathbf{G} , to achieve the ℓ_0 regularization (the number of zero elements in theory in \mathbf{G} is n_e ; established in Sections 3.1).

After the noisy data are generated, we run a regular GLM to obtain an updated estimate $\mathcal{B}^{(t)}$ by minimizing the loss function formulated given the noise-augmented data, which is

$$\begin{aligned} l_{na}^{(t)} &= l(\mathcal{B}, \phi | \mathbf{y}_i, \mathcal{X}_i, e_{y,j}^{(t)}, \mathcal{Z}_j^{(t)}, 1 \leq i \leq n, 1 \leq j \leq n_e) \\ &= -\sum_{i=1}^n \ln p(y_i | \mathcal{X}_i, \mathcal{B}, \phi) - \sum_{j=1}^{n_e} \ln p(e_{y,j}^{(t)} | \mathcal{Z}_j^{(t)}, \mathcal{B}, \phi). \end{aligned} \quad (10)$$

This step can leverage any software that runs regular GLM (without regularization) without a need to design or code an optimization procedure to estimate \mathcal{B} .

In what follows, we establish theoretically that NA_0CT^2 achieves ℓ_0 regularization on the core tensor \mathcal{G} upon convergence and provide some intuition on how that is achieved. We first examine linear TR with Gaussian Y (Section 3.1) and then extend the conclusion to GLM TR in general (Section 3.2).

3.1 ℓ_0 regularization via NA_0CT^2 in Linear TR

In linear TR, the loss function is the ℓ_2 loss. Given observed data (\mathcal{X}_i, y_i) for $i = 1, \dots, n$ and noisy data $(\mathcal{Z}_j, e_{y,j} \equiv d)$ for $j = 1, \dots, n_e$ that augment the former, the loss function is

$$\begin{aligned} l_{na} &= \sum_{i=1}^n (y_i - \langle \mathcal{X}_i, \mathcal{B} \rangle)^2 + \sum_{j=1}^{n_e} (e_{y,j} - \langle \mathcal{Z}_j, \mathcal{B} \rangle)^2 \\ &= \sum_{i=1}^n (y_i - \langle \mathcal{X}_i, \mathcal{B} \rangle)^2 + n_e d^2 - 2d \sum_{j=1}^{n_e} \langle \mathcal{Z}_j, \mathcal{B} \rangle + \sum_{j=1}^{n_e} \langle \mathcal{Z}_j, \mathcal{B} \rangle^2. \end{aligned} \quad (11)$$

Eq (11) contains both a linear term and a quadratic term in \mathcal{B} . We show below that it is the quadratic term that yields ℓ_0 regularization. Toward that end, augmented noisy data need to be designed in a way such that the linear term is zero so to avoid any undesirable regularization effect on \mathcal{B} from the linear term. In the linear TR case, there are two ways to achieve the goal. First, we can set $e_{y,j} \equiv 0$ for all $j = 1, \dots, n_e$, in which case, the linear term $2d \sum_{j=1}^{n_e} \langle \mathcal{Z}_j, \mathcal{B} \rangle = 0$ in Eq (11). Second, we generate two blocks of noisy terms, each of size n_e . The first n_e terms contain noisy data points $(e_{y,j}, \mathcal{Z}_j)$ for $1 \leq j \leq n_e$ and the second block contains data points $(e_{y,j} = e_{y,j-n_e}, \mathcal{Z}_j = -\mathcal{Z}_{j-n_e})$ for $n_e + 1 \leq j \leq 2n_e$, as demonstrated in Eq (12),

$$\begin{bmatrix} (\mathcal{X}_i, y_i)_{i=1, \dots, n} \\ (\mathcal{Z}_j^{(t)}, e_{y,j}^{(t)})_{j=1, \dots, 2n_e} \end{bmatrix} = \begin{bmatrix} (\mathcal{X}_i, y_i)_{i=1, \dots, n} \\ (\mathcal{Z}_j^{(t)}, e_{y,j}^{(t)})_{j=1, \dots, n_e} \\ (-\mathcal{Z}_j^{(t)}, e_{y,j}^{(t)})_{j=1, \dots, n_e} \end{bmatrix}. \quad (12)$$

The linear term in Eq (11) is also 0 as $\sum_{j=1}^{n_e} \langle \mathcal{Z}_j, \mathcal{B} \rangle + \sum_{j=n_e+1}^{2n_e} \langle \mathcal{Z}_j, \mathcal{B} \rangle = 0$ per the design in Eq (12). In summary, both noise augmentation schemes lead to

$$l_{na} = \sum_{i=1}^n (y_i - \langle \mathcal{X}_i, \mathcal{B} \rangle)^2 + C_1 \sum_{j=1}^{n_e} \langle \mathcal{Z}_j, \mathcal{B} \rangle^2 + C_2, \quad (13)$$

where $C_1 = 1, C_2 = 0$ if we set $e_{y,j} \equiv 0$ and $C_1 = 2, C_2 = 2n_e d^2$ if we use the two-block noise augmentation scheme.

We now show the quadratic term $\sum_{j=1}^{n_e} \langle \mathcal{Z}_j, \mathcal{B} \rangle^2$ in Eq (13) leads to ℓ_0 regularization on the core tensor of \mathcal{B} if Tucker decomposition is applied to \mathcal{Z} and \mathcal{B} . The inner product $\langle \mathcal{Z}_j, \mathcal{B} \rangle$ in Eq (13), after Tucker decomposition on \mathcal{B} and given how \mathcal{Z} is designed, can be written as

$$\begin{aligned} & \left\langle \sum_{i_1=1}^{R_1} \sum_{i_2=1}^{R_2} \cdots \sum_{i_D=1}^{R_D} e_{j,i_1 i_2 \dots i_D} \mathbf{u}_1^{i_1} \circ \mathbf{u}_2^{i_2} \circ \cdots \circ \mathbf{u}_D^{i_D}, \sum_{i_1=1}^{R_1} \sum_{i_2=1}^{R_2} \cdots \sum_{i_D=1}^{R_D} g_{i_1 i_2 \dots i_D} \mathbf{u}_1^{i_1} \circ \mathbf{u}_2^{i_2} \circ \cdots \circ \mathbf{u}_D^{i_D} \right\rangle \\ &= \sum_{i_1=1}^{R_1} \sum_{i_2=1}^{R_2} \cdots \sum_{i_D=1}^{R_D} \langle e_{j,i_1 i_2 \dots i_D} \mathbf{u}_1^{i_1} \circ \mathbf{u}_2^{i_2} \circ \cdots \circ \mathbf{u}_D^{i_D}, g_{i_1 i_2 \dots i_D} \mathbf{u}_1^{i_1} \circ \mathbf{u}_2^{i_2} \circ \cdots \circ \mathbf{u}_D^{i_D} \rangle + \\ & \quad \sum_{i_d \neq j_d, 1 \leq i_d, j_d \leq R_d} \langle e_{j,i_1 i_2 \dots i_D} \mathbf{u}_1^{i_1} \circ \mathbf{u}_2^{i_2} \circ \cdots \circ \mathbf{u}_D^{i_D}, g_{j_1 i_2 \dots j_D} \mathbf{u}_1^{j_1} \circ \mathbf{u}_2^{j_2} \circ \cdots \circ \mathbf{u}_D^{j_D} \rangle \end{aligned} \quad (14)$$

$$= \sum_{i_1=1}^{R_1} \sum_{i_2=1}^{R_2} \cdots \sum_{i_D=1}^{R_D} e_{j,i_1 i_2 \dots i_D} g_{i_1 i_2 \dots i_D}, \quad (15)$$

Eq (15) holds due to the orthonormality of the columns in \mathbf{u}_d (thus $\langle \mathbf{u}_1^{i_1} \circ \mathbf{u}_2^{i_2} \circ \cdots \circ \mathbf{u}_D^{i_D}, \mathbf{u}_1^{i_1} \circ \mathbf{u}_2^{i_2} \circ \cdots \circ \mathbf{u}_D^{i_D} \rangle = 1$ in the first term and the second term in Eq (14) is zero). Substituting $\langle \mathcal{Z}_j, \mathcal{B} \rangle$ in Eq (13) with Eq (15), we have

$$l_{na} = \sum_{i=1}^n (y_i - \langle \mathcal{X}_i, \mathcal{B} \rangle)^2 + C_1 \sum_{j=1}^{n_e} \left(\sum_{i_1=1}^{R_1} \sum_{i_2=1}^{R_2} \cdots \sum_{i_D=1}^{R_D} g_{i_1 i_2 \dots i_D} e_{j,i_1 i_2 \dots i_D} \right)^2 + C_2 \quad (16)$$

$$= \sum_{i=1}^n (y_i - \langle \mathcal{X}_i, \mathcal{B} \rangle)^2 + \lambda \sum_{j=1}^{n_e} \left(\sum_{i_1=1}^{R_1} \sum_{i_2=1}^{R_2} \cdots \sum_{i_D=1}^{R_D} g_{i_1 i_2 \dots i_D} e'_{j,i_1 i_2 \dots i_D} \right)^2 + C_2, \quad (17)$$

$$\text{where } e'_{j,i_1 i_2 \dots i_D} = \lambda^{-1/2} e_{j,i_1 i_2 \dots i_D} \sim \mathcal{N}(0, g_{i_1 i_2 \dots i_D}^{-2}). \quad (18)$$

Eq (17) suggests that the second term of the loss function formulated on augmented noisy data serves as a regularization term on the core tensor \mathcal{G} of \mathcal{B} .

The key to understand methodologically and intuitively why NA₀CT² with the carefully constructed data augmentation scheme achieves ℓ_0 regularization is to realize that the optimization problem in Eq (17) is the dual problem to and the Lagrange expression of the primal constrained optimization problem in Eq (19) with the same multiplier λ used for all

n_e constrained terms;

$$\begin{aligned}
& \min_{\mathcal{B}} \sum_{i=1}^n (y_i - \langle \mathcal{X}_i, \mathcal{B} \rangle)^2, \text{ subject to} \\
& \sum_{i_1=1}^{R_1} \sum_{i_2=1}^{R_2} \cdots \sum_{i_D=1}^{R_D} g_{i_1 i_2 \dots i_D} e'_{1, i_1 i_2 \dots i_D} = 0 \\
& \sum_{i_1=1}^{R_1} \sum_{i_2=1}^{R_2} \cdots \sum_{i_D=1}^{R_D} g_{i_1 i_2 \dots i_D} e'_{2, i_1 i_2 \dots i_D} = 0, \\
& \vdots \\
& \sum_{i_1=1}^{R_1} \sum_{i_2=1}^{R_2} \cdots \sum_{i_D=1}^{R_D} g_{i_1 i_2 \dots i_D} e'_{n_e, i_1 i_2 \dots i_D} = 0.
\end{aligned} \tag{19}$$

Eq (19) shows that the n_e linear constraints in the primal problem promote orthogonality between the core tensor elements g 's and augmented noisy tensor predictors. With $n_e < p$, the n_e constraints only affect a subset of the p parameters. In each iteration of the NA₀CT² algorithm with a new set of n_e noisy samples, the fix subset comprising of the n observed samples is responsible for learning the relationship (the GLM coefficients) between the predictors \mathbf{X} and the response Y while the noisy subset drives the estimates of parameters g 's to be orthogonal to the hyper plane spanned by the n_e noisy predictor vectors because that's when the loss constructed on the noisy data subset in Eq (17) is minimized. Per the design of the noise generation distribution, the smaller magnitude a g is of, the larger the variance of the noise-generating distribution, and the more dispersed the noisy predictor corresponding to that g is and the less relevant it is for the prediction of Y in the TR model, further pushing the estimated value of g towards zero, until stabilization and convergence.

Proposition 1 states the constrained optimization Eqn (19) is ℓ_0 regularization with exactly n_e elements in \mathcal{G} set at 0. The proof is straightforward. There are n_e linear constraints on the elements g 's of in \mathcal{G} in Eqn (19), the coefficients of which are noise terms drawn independently from the noise-generating distribution, implying that exactly n_e entries can be expressed exactly as a linear function of the rest of the components in \mathcal{G} ; in other words, n_e components in the core tensor can be set at 0.

Proposition 1 (ℓ_0 regularization on core tensor in linear TR through NA₀CT²). The constrained optimization problem in Eqn (19) is equivalent to

$$\begin{aligned}
& \min_{\mathcal{B}} \sum_{i=1}^n (y_i - \langle \mathcal{X}_i, \mathcal{B} \rangle)^2 \\
& \text{subject to } \sum_{i_1=1}^{R_1} \sum_{i_2=1}^{R_2} \cdots \sum_{i_D=1}^{R_D} \mathbb{1}(g_{i_1 i_2 \dots i_D} = 0) = n_e.
\end{aligned} \tag{20}$$

Since $g_{i_1 i_2 \dots i_D}$ is unknown, the iterative NA₀CT² procedure would require users to supply an initial $\mathcal{B}^{(0)}$ and then use the estimates of \mathcal{G} from the previous iteration when sampling noisy tensor predictor data in Eq (9). Upon convergence, the estimate of \mathcal{G} stabilizes, and so is the noise-generating distribution; but the random fluctuation in the estimate of \mathcal{G} still exists from iteration to iteration given that randomly sampled noisy data are different across the iterations. For that reason, while the ℓ_0 regularization via NA₀CT² is exact conceptually, the realized regularization in actual implementations of NA₀CT² would only get arbitrarily close to ℓ_0 due to the random fluctuation. One way to mitigate the numerical randomness

around the estimate of \mathcal{B} so to get as close as possible to exact ℓ_0 is to take the average of estimated parameters over multiple iterations upon convergence; details are provided in Algorithm 1 of Section 3.3.

3.2 ℓ_0 regularization via NA₀CT² in GLM TR

When Y follows an exponential family distribution in Eq (1), the loss function can be formulated as a negative log-likelihood. We employ the same noisy-data augmentation scheme as in Eq (12) with the two blocks of noisy data, each of size n_e with opposite signs on the noisy predictor tensor when augmenting the loss function for NA₀CT²; that is,

$$\begin{aligned} l_{na}(\mathcal{B}, \phi | y_i, \mathcal{X}_i, e_{y,j}, \mathcal{Z}_j, 1 \leq i \leq n, 1 \leq j \leq 2n_e) \\ = - \sum_{i=1}^n \ln p(y_i | \mathcal{X}_i, \mathcal{B}, \phi) - \sum_{j=1}^{n_e} \ln p(e_{y,j} | \mathcal{Z}_j, \mathcal{B}, \phi) - \sum_{j=n_e+1}^{2n_e} \ln p(e_{y,j} | -\mathcal{Z}_j, \mathcal{B}, \phi). \end{aligned} \quad (21)$$

Proposition 2 (ℓ_0 regularization on core tensor in general TR through NA₀CT²). Minimization of the augment loss function in Eqn (21) is equivalent to

$$\begin{aligned} \min_{\mathcal{B}} - \sum_{i=1}^n \ln p(y_i | \mathcal{X}_i, \mathcal{B}, \phi) \\ \text{subject to } \sum_{i_1=1}^{R_1} \sum_{i_2=1}^{R_2} \cdots \sum_{i_D=1}^{R_D} \mathbb{1}(g_{i_1 i_2 \dots i_D} = 0) = n_e. \end{aligned} \quad (22)$$

Propositions 2 is proved as follows. Applying the Taylor expansion around $\langle \mathcal{Z}_j, \mathcal{B} \rangle = 0$, l_{na} in Eq (21) becomes

$$\begin{aligned} & - \sum_{i=1}^n \ln p(y_i | \mathcal{X}_i, \mathcal{B}, \phi) - \sum_{j=1}^{n_e} \left\{ \frac{-B(0)}{a(\phi)} + h(e_{y,j}, \phi) + \frac{e_{y,j} - B'(0)}{a(\phi)} \langle \mathcal{Z}_j, \mathcal{B} \rangle + \frac{B''(0)}{2a(\phi)} \langle \mathcal{Z}_j, \mathcal{B} \rangle^2 \right. \\ & + \left. O(\langle \mathcal{Z}_j, \mathcal{B} \rangle^3) + O(\langle \mathcal{Z}_j, \mathcal{B} \rangle^4) + \dots \right\} - \sum_{j=n_e+1}^{2n_e} \left\{ \frac{-B(0)}{a(\phi)} + h(e_{y,j}, \phi) + \frac{e_{y,j} - B'(0)}{a(\phi)} \langle -\mathcal{Z}_j, \mathcal{B} \rangle \right. \\ & + \left. \frac{B''(0)}{2a(\phi)} \langle -\mathcal{Z}_j, \mathcal{B} \rangle^2 + O(\langle -\mathcal{Z}_j, \mathcal{B} \rangle^3) + O(\langle -\mathcal{Z}_j, \mathcal{B} \rangle^4) + \dots \right\} \\ & = - \sum_{i=1}^n \ln p(y_i | \mathcal{X}_i, \mathcal{B}, \phi) + C_1 \sum_{j=1}^{n_e} \sum_{l=1}^{\infty} \langle \mathcal{Z}_j, \mathcal{B} \rangle^{2l} + C_2, \end{aligned} \quad (23)$$

where $C_1 = -B''(0)/a(\phi)$ and $C_2 = 2n_e B(0)/a(\phi) - \sum_{j=1}^{2n_e} h(e_{y,j}, \phi)$ are constant independent of \mathcal{B} . The augmented loss function in Eq (23) compared to the the regularization term in Eq (13) in linear TR, has additional even exponents of $\langle \mathcal{Z}_j, \mathcal{B} \rangle$ in addition to the quadratic term $\langle \mathcal{Z}_j, \mathcal{B} \rangle^{2l}$. These additional even-powered terms of $\langle \mathcal{Z}_j, \mathcal{B} \rangle$ have the same regularization effect as the quadratic term, which is orthogonality constraints between \mathbf{e}_j and the core tensor \mathcal{G} or the ℓ_0 regularization on \mathcal{G} just as in the case of linear TR. Therefore, the statements from Propositions 1 also apply to the GLM TR setting,

3.3 Algorithm for NA₀CT²

Algorithm 1: The NA₀CT² procedure

input : observed data (\mathcal{X}_i, y_i) for $i = 1, \dots, n$; noisy data size n_e , noisy response data $e_{y,j}$ for $j = 1, \dots, n_e$; regularization hyperparameter λ ; maximum iterations T ; stopping thresholds τ or η ; zero threshold τ_0 , moving average window m ; dimension of core tensor $\mathcal{G} : R_1 \times R_2 \times \dots \times R_D$ if applicable (optional)

output: TR coefficient tensor $\hat{\mathcal{B}}$

- 1 Standardize \mathcal{X}_i for each $1 \leq i \leq n$;
- 2 Calculate $\hat{\mathcal{B}}$ from regression model on Y on vectorized \mathcal{X}_i and set $\bar{\mathcal{B}}^{(0)} = \hat{\mathcal{B}}^{(0)} = \hat{\mathcal{B}}$;
- 3 $t \leftarrow 1$, convergence status $s \leftarrow 0$;
- 4 **while** $t \leq T$ and $s = 0$ **do**
- 5 Apply Tucker decomposition to $\hat{\mathcal{B}}^{(t-1)} = \hat{\mathcal{G}}^{(t-1)} \times_1 \hat{\mathbf{U}}_1^{(t-1)} \times_2 \hat{\mathbf{U}}_2^{(t-1)} \times_3 \dots \times_D \hat{\mathbf{U}}_D^{(t-1)}$;
- 6 **if** $t \leq m$ **then**
- 7 $\bar{\mathcal{G}}^{(t-1)} \leftarrow \hat{\mathcal{G}}^{(t-1)}$;
- 8 **else**
- 9 $\bar{\mathcal{G}}^{(t-1)} \leftarrow \{ \sum_{i=t-m-1}^t \hat{\mathcal{G}}^{(i)} / m + c \}$;
- 10 // c is a small constant (e.g., 10^{-7}) to avoid overflow of $(\bar{\mathcal{G}}^{(t-1)})^{-2}$.
- 10 **end**
- 11 Generate elements in the core tensor $\mathcal{E}_j^{(t)}$ of the noisy predictor \mathcal{Z}_j :
 $e_{j,i_1 i_2 \dots i_D} \sim \mathcal{N}(0, \lambda (\bar{g}_{i_1 i_2 \dots i_D}^{(t-1)})^{-2})$ for $j = 1, \dots, n_e$, $i_d = 1, \dots, R_d$, and $d = 1, \dots, D$;
- 12 Calculate $\mathcal{Z}_j = \mathcal{E}_j^{(t)} \times_1 \hat{\mathbf{U}}_1^{(t-1)} \times_2 \hat{\mathbf{U}}_2^{(t-1)} \times_3 \dots \times_D \hat{\mathbf{U}}_D^{(t-1)}$ for $j = 1, \dots, n_e$;
- 13 Combine $(\mathcal{X}_i, y_i)_{i=1, \dots, n}$, $(\mathcal{Z}_j^{(t)}, e_{y,j})_{j=1, \dots, n_e}$, and $(-\mathcal{Z}_j^{(t)}, e_{y,j})_{j=1, \dots, n_e}$ to form an augmented dataset of size $n + 2n_e$;
- 14 Run GLM on the augmented data with vectorized predictor
 $\text{vec}(\mathcal{X}_i, \mathcal{Z}_j^{(t)})_{i=1, \dots, n; j=1, \dots, 2n_e}$ and response $(y_i, e_{y,j})_{i=1, \dots, n; j=1, \dots, 2n_e}$ to obtain updated estimate $\hat{\mathcal{B}}^{(t)}$;
- 15 **if** $t \leq m$ **then**
- 16 $\bar{\mathcal{B}}^{(t)} \leftarrow \hat{\mathcal{B}}^{(t)}$ and $\bar{l}^{(t)} \leftarrow \hat{l}(\hat{\mathcal{B}}^{(t)})$;
- 17 **else**
- 18 $\bar{\mathcal{B}}^{(t)} \leftarrow \sum_{i=t-m-1}^t \hat{\mathcal{B}}^{(i)} / m$ and $\bar{l}^{(t)} \leftarrow \sum_{i=t-m-1}^t \hat{l}(\hat{\mathcal{B}}^{(i)}) / m$;
- 19 **end**
- 20 **if** $|\bar{l}^{(t)} - \bar{l}^{(t-1)}| \leq \tau$ or $\|\bar{\mathcal{B}}^{(t)} - \bar{\mathcal{B}}^{(t-1)}\|_1 \leq \eta$ **then**
- 21 $s = 1$;
- 22 **end**
- 23 $t \leftarrow t + 1$;
- 24 **end**
- 25 Output $\bar{\mathcal{B}}^{(t)}$. // the next two steps are optional
- 26 Apply Tucker decomposition to $\bar{\mathcal{B}}^{(t)}$ to obtain $\hat{\mathcal{G}} \times_1 \hat{\mathbf{U}}_1 \times_2 \hat{\mathbf{U}}_2 \times_3 \dots \times_D \hat{\mathbf{U}}_D$, replace any element in $\hat{\mathcal{G}}$ that is $\leq \tau_0$ with 0 to obtain a new \mathcal{G}_0 ;
- 27 Output $\hat{\mathcal{B}} = \hat{\mathcal{G}}_0 \times_1 \hat{\mathbf{U}}_1 \times_2 \hat{\mathbf{U}}_2 \times_3 \dots \times_D \hat{\mathbf{U}}_D$.

Algorithm 1 lists the steps for running the NA₀CT² procedure. The algorithm uses an explicitly specified stopping criterion. Besides that, plotting trace plots of loss functions

to eyeball the convergence or examine the change in the estimate of $\hat{\mathcal{B}}$ across iterations such as $\|\bar{\mathcal{B}}^{(t)} - \bar{\mathcal{B}}^{(t-1)}\|_1 \leq \eta$, where η is a small constant, can also be used to evaluate convergence. Users need to supply an initial set of parameters, such as from the regression model on vectorized \mathcal{X}_i , which can be regularized or not, as given in line 2. The algorithm also includes a moving window $m > 1$ to help to smooth out the randomness in the estimated tensor $\hat{\mathcal{B}}$ and in the loss function since augmented noisy data change at every iteration. The usage of m is algorithmic and doesn't affect the theoretical property of NA₀CT² established in Proposition 1. Since the variances of noise-generating Gaussian distributions are inversely proportional to the squared core tensor entry values, the estimates of zero-valued entries in the core tensor via NA₀CT² would shrink toward 0 upon the convergence of the algorithm, leading to very large variances in the noise-generating distributions and potential overflows when running the algorithm. To avoid this, we recommend lower bounding the estimated elements in the core tensor by a very small constant τ_0 (e.g., 10^{-10}).

3.3.1 Choice of hyperparameters

The two hyperparameters in the loss function of NA₀CT² λ and n_e both affect the number of estimated zeros in the core tensor and can be tuned via cross-validation (CV) with metrics such as information criteria (e.g., AIC) from GLMs. First, to achieve the ℓ_0 regularization on the core tensor, n_e should be set at a value smaller than p , the product of the dimensionalities of the core tensor. Second, our empirical studies suggest that 1) small λ may not yield enough sparsity even when n_e is larger than the true number of zero n_e and close to p ; 2) when λ is large, the estimated number of zeros in the core tensor is roughly equal to the value of n_e when $n_e \leq n_0$ and increases with n_e for $n_e > n_0$; 3) when λ is not small or too large, the estimated number of zeroes in the core tensor increases with n_e and reaches a plateau valued at n_0 . In other words, with an appropriate chosen λ , the estimated number of zeros would be robust to the choice of n_e and equals to n_0 (see Appendix B for an empirical demonstration).

Before providing a recommendation on the choice m , we first provide the rationale for having a moving window of size m . Algorithmically, averaging over m iterations helps smooth the parameter estimates, improving and accelerating the the algorithm's convergence, especially considering every iterations is based on a different augmented dataset. More importantly, m is more than just an algorithmic parameter to define a smoothing window. As shown in Li and Liu (2022), theoretically, it would require $m \rightarrow \infty$ to achieve the almost sure (a. s.) convergence of loss function given the noise-augmented data to its expectation and the a. s. convergence of the minimizer of the former to the minimizer of the latter when fixed $n_e \leq p$. This implies that in practical application of this algorithm, a large number of m would be needed. Besides, the noisy-data augmentation regularization with a fixed n_e also exhibits ensemble learning behavior upon convergence, where the model trained on each of the m augmented datasets is a weak learner, generating the diversity among the final estimates of the model parameters, which are averages over the m sets. With an understanding of the functionality of m , we recommend selecting a relatively large value of m , factoring in the complexity of the problem. We run some experiments to examine how m affects the convergence of the NA₀CT² algorithm and the results are presented in Appendix A. As expected, a larger m would lead to better convergence in terms of more

stabilized loss function with less fluctuation and smaller loss values given its implicit ensemble learning behavior. We may also adaptively tune m after the algorithm starts by monitoring the residual deviance. If noticeable divergence or fluctuations occurs with the preset m , increasing it can help achieve stable convergence.

The input of the dimension of \mathcal{G} in Algorithm 1 is optional and depends on whether there is prior information to inform the sparsity and dimensionality of \mathcal{G} relative to \mathcal{B} . If no such prior information exists, dimension of \mathcal{G} is set to be the same as \mathcal{B} by default. If there is prior information on the dimensions of one or more modes of \mathcal{B} , one may set that mode at the smaller dimension(s) accordingly, incorporating the prior knowledge and also helping reduce the computational cost later on when running the algorithm.

Note that setting the \mathcal{G} at a smaller dimension than \mathcal{B} , running tensor regression without regularization, and constructing \mathcal{B} per Eqn (2) (referred as *smaller-core-tensor without regularization* or *SCOT-WOR* for brevity) does not have quite the same sparsity effect as imposing the ℓ_0 constraint via Algorithm 1, though there is some overlap. Specifically, there are a couple of key differences between the two approaches. First, *SCOT-WOR* would need to tune/specify D hyperparameters (i.e., $R_1 \times \dots \times R_D$) whereas NA_0CT^2 only tune hyperparameters λ and n_e . If grid search is used to tune R_1, \dots, R_D in *SCOT-WOR*, it can be computationally costly as there are $\prod_{d=1}^D k_d$ possible scenarios to choose from, where k_d is the dimensionality of the grid for R_d . In contrast, NA_0CT^2 has only two hyperparameters n_e and λ and it is robust to the value of n_e in that the correct number (n_0) of structural 0's in \mathcal{G} can be learned for a wide range of $n_e \in [n_0, p]$ for a given proper λ value. Second, by pre-specifying R_1, \dots, R_D , the structure of \mathcal{G} is set, lacking the flexibility that NA_0CT^2 offers to \mathcal{G} on its structure – that is, the locations of the non-zero elements in \mathcal{G} is completely data driven without following a pre-specified pattern. In some sense, NA_0CT^2 can be viewed as naturally incorporating *SCOT-WOR* because $R_d \leq I_d$ in Eqn (2), where $I_1 \times \dots \times I_D$ is the dimensionality of \mathcal{B} . In practice, one can set \mathcal{G} with $R_d \leq I_d$ for $d = 1, \dots, D$ in a confident but conservative manner (e.g., if $I_1 = 50$, $R_1 = 45$ based on some prior knowledge), and then run Algorithm 1 to impose further sparsity constraints on \mathcal{G} . This approach is not only more computationally efficient with a smaller \mathcal{G} to estimate but also leverages the flexibility the noise-augmented ℓ_0 regularization NA_0CT^2 offers to its structure.

3.3.2 Time complexity

The time complexity of Algorithm 1 can be analyzed by breaking down the major steps and examining the time complexity of each step, as presented in Table 2. In summary, the time complexity is cubic in the dimensionality \mathcal{B} ($I_1 \times \dots \times I_D$) and \mathcal{G} ($R_1 \times \dots \times R_D$) and linear in $T \cdot (n + n_e)$.

4 Numerical Examples

We apply NA_0CT^2 in five numerical examples (Table 3). The first three examples use simulated data on three different types of responses (Gaussian, binary, count), and the two examples are on real-life datasets with continuous and binary responses respectively. We compare NA_0CT^2 with the following competing regression approaches in outcome prediction

Table 2: Time complexity of the key steps in Algorithm 1

	line in Algorithm 1	time complexity
every	5: Tucker decomposition of $\hat{\mathcal{B}}^{(t-1)}$	$O\left(\sum_{t=1}^T T_{\text{tucker}}^{(t-1)} \left(pD + \sum_{d=1}^D I_d R_d \prod_{j \neq d} R_j\right)\right)^\dagger$
iteration	12: Calculation of \mathcal{Z}_j	$O\left(T n_e \sum_{j=1}^D I_j R_j \prod_{j' \neq d} R_{j'}\right)^\ddagger$
t	14: GLM on the augmented data	$O\left(\sum_{t=1}^T T_{\text{glm}}^{(t)} (p^2(n + 2n_e) + p^3)\right)^\ddagger$
one	26: Tucker decomposition of $\bar{\mathcal{B}}^{(t)}$	$O\left(T'_{\text{tucker}} \left(pD + \sum_{d=1}^D I_d R_d \prod_{j \neq d} R_j\right)\right)^\dagger$
time	27: calculation of $\hat{\mathcal{B}}$	$O\left(\sum_{j=1}^D I_j R_j \prod_{j' \neq d} R_{j'}\right)^\ddagger$
total: $O\left(\left(\sum_{t=1}^T T_{\text{tucker}}^{(t-1)} + T'_{\text{tucker}}\right) \cdot \left(pD + \sum_{d=1}^D I_d R_d \prod_{j \neq d} R_j\right)\right) + O\left((T n_e + 1) \sum_{j=1}^D I_j R_j \prod_{j' \neq d} R_{j'}\right) + O\left(\sum_{t=1}^T T_{\text{glm}}^{(t)} (p^2(n + 2n_e) + p^3)\right)$, where $p = \prod_{d=1}^D I_d$.		

[†] based on the Higher-Order Orthogonal Iteration (HOOI) algorithm for Tucker decomposition (e.g., used by the `tucker` function in `rTensor` in R). $T_{\text{tucker}}^{(t-1)}$ is the number of iterations for HOOI to convergence in iteration t as it is an iterative algorithm itself. $T_{\text{tucker}}^{(t-1)}$ depends on the convergence criteria; for R function `tucker`, the default options are `max_iter = 25`, `tol = 1e-05`.

[‡] based on Iteratively Reweighted Least Squares (IRLS) (e.g. used by R function `glm`). $T_{\text{glm}}^{(t)}$ is the number of iterations to convergence and depends on convergence criteria; for R function `glm`, the default options are `max_iter=25`, `tol=1e-08`.

in all examples and also examine the ability of feature selection in each method in the real data examples.

- GLM on vectorized predictors $\text{vec}(\mathcal{X})$, unregularized and with ℓ_1 regularization.
- TR with CP decomposition on \mathcal{B} , unregularized and with ℓ_2 regularization on the entries \mathbf{U}_d for $d = 1, 2, \dots, D$ of \mathcal{B} after decomposed (Eq (3)) (Zhou et al., 2013).
- TR with Tucker decomposition on \mathcal{B} , unregularized and with sparsity (e.g. ℓ_1) regularization on the core tensor (Li et al., 2018).
- Bayesian GLM on vectorized predictors $\text{vec}(\mathcal{X})$ with the spike-and-slab prior on model coefficients in the simulation studies.
- SVM in logistic TR in the simulation studies.
- NA_0CT^2 (our method): TR with Tucker decomposition on \mathcal{B} and ℓ_0 -regularization on the core tensor.

To make the TR models based on Tucker decomposition and CP decomposition comparable, we set the numbers of free parameters roughly the same in these two types of TR models. We first set the dimensionality of the core tensor in the Tucker decomposition and calculated the total number of parameters according to Table 1. We then back-calculated the dimensionality R in the CP decomposition that yields the same or a similar number of parameters as with Tucker decomposition. The numbers of parameters in each model are listed in Table 3 for the 4 examples. Though the number of parameters in the Tucker and CP decomposition-based TR in the 3 simulation studies are the same as the GLM on $\text{vec}(\mathcal{X})$, the former two explore and leverage the structural information in tensor data and are expected to provide better prediction results.

Table 3: Number parameters of different methods in the examples

study	Tucker	CP	GLM on $\text{vec}(\mathcal{X})$
3 simulation studies	64	60	64
	$(R_1 = R_2 = R_3 = 4)$	$(R = 6)$	$(I_1 = I_2 = I_3 = 4)$
FG-NET	825	825	841
	$(R_1 = R_2 = 25)$	$(R = 25)$	$(I_1 = I_2 = 29)$
KTH	64	60	64
	$(R_1 = R_2 = R_3 = 4)$	$(R = 6)$	$(I_1 = I_2 = I_3 = 4)$

The dimensions R_1 and R_2 in the Tucker decomposition in the FG-NET applications were chosen by cross-validation.

4.1 Simulation Studies

We examine three response types Y in the simulation studies – Gaussian, binary, and count; and run linear, logistic, and Poisson TR, respectively, each case given a tensor predictor \mathcal{X} . Respond data \mathbf{y} were generated from $\mathcal{N}(\langle \mathcal{X}, \mathcal{B} \rangle, 0.5^2)$ and data on \mathcal{X} were generated from $\mathcal{N}(0, 1)$ in the linear TR case, $Y \sim \text{Bern}((1 + e^{-\langle \mathcal{B}, \mathcal{X} \rangle})^{-1})$ and data on \mathcal{X} were generated from $\mathcal{N}(0, 0.25^2)$ in the logistic TR case, and $Y \sim \text{Poisson}(e^{\langle \mathcal{B}, \mathcal{X} \rangle})$ and \mathcal{X} were generated from $-2|\mathcal{N}(0.1, 0.3^2)| + 0.6$ in the Poisson case. Both \mathcal{B} and \mathcal{X} are of dimension $4 \times 4 \times 4$. Elements in \mathcal{B} were randomly generated from a certain distribution and were then adjusted to result in a sparse core tensor in the Tucker decomposition. Specifically, in the linear and logistic cases, 8 elements of \mathcal{B} were first generated from $\mathcal{N}(0, 1)$, then were copied 8 times to formulate \mathcal{B} . The set-up of \mathcal{B} in the Poisson case was similar with the only difference being that the 8 elements of \mathcal{B} were generated from $\text{unif}(0, 0.3)$. In all regression cases, this way of constructing \mathcal{B} leads to 2 non-zero elements and 62 zero elements in the core tensor after the Tucker decomposition. The sample size n of each training dataset was set at $n = 300$ for the linear case, $n = 300$ for the binary case, and $n = 200$ for the Poisson case. The size of each testing dataset was set to 200.

For NA_0CT^2 , we set $n_e = 62$, $\lambda = 50$, $T = 30000$, $m = 600$, $\tau_0 = 10^{-6}$, $\tau = 0.01$ in the linear TR; $n_e = 62$, $\lambda = 50$, $T = 5000$, $m = 600$, $\tau_0 = 10^{-6}$, $\tau = 0.01$ in the logistic TR; and $n_e = 62$, $\lambda = 50$, $T = 10000$, $m = 600$, $\tau_0 = 10^{-6}$, $\tau = 0.01$ in the Poisson TR.

The TR models based on Tucker decomposition (Li et al., 2018) use an iterative block relaxation algorithm to estimate the parameters (Algorithm 2). Estimation of each “block” of parameters given the rest parameters in each iteration is equivalent to running a GLM. The objective function l on lines 5 and 7 is the log-likelihood. Two different TR models were run – with and without ℓ_1 regularization when estimating the core tensor. R package `glmnet` was used to run Algorithm 2. The hyperparameter for the ℓ_1 regularization was set at 10^{-3} in the Poisson TR model (`cv.glmnet` resulted in errors) and was chosen by 5-fold cross-validation (CV) in the other cases.

The TR models based on the CP decomposition (Zhou et al., 2013) used the same iterative block relaxation algorithm to estimate the parameters (Algorithm 3). Two different TR models were run – with and without the ℓ_2 regularization when estimating \mathbf{U}_d for $d = 1, 2, \dots, D$ in Eq (3). The hyperparameter for the ℓ_2 regularization was chosen by 5-fold CV.

For the Bayesian GLM with the spike-and-slab prior, we used R package `BoomSpikeSlab` and performed a 5-fold CV to select the optimal values for the expected model size (number non-

zero elements in \mathcal{B}) out of $\{5, 10, 15\}$ (`expected.model.size`) and the weight assigned to the prior estimates of the model parameters (`prior.information.weight`) out of $\{0.1, 0.5, 0.9\}$.

Algorithm 2: TR based on Tucker decomposition (Li et al., 2018)

input : data (\mathcal{X}_i, y_i) for $i = 1, \dots, n$; iterations T ; stopping threshold η
output: estimated coefficient tensor $\hat{\mathcal{B}}$

- 1 Initialize $\hat{\mathcal{G}}^{(0)} \in \mathbb{R}^{R_1 \times R_2 \times \dots \times R_D}$ and $\hat{\mathbf{U}}_d^{(0)} \in \mathbb{R}^{I_d \times R_d}$ for $d = 1, 2, \dots, D$;
- 2 $t \leftarrow 1$, convergence status $s \leftarrow 0$;
- 3 **while** $t \leq T$ and $s = 0$ **do**
- 4 **for** $d = 1$ to D **do**
- 5 $\hat{\mathbf{U}}_d^{(t)} = \operatorname{argmax}_{\mathbf{U}_d} \sum_{i=1}^n l(\hat{\mathcal{G}}^{(t-1)}, \hat{\mathbf{U}}_1^{(t)}, \dots, \hat{\mathbf{U}}_{d-1}^{(t)}, \mathbf{U}_d, \hat{\mathbf{U}}_{d+1}^{(t-1)}, \dots, \hat{\mathbf{U}}_D^{(t-1)} | y_i, \mathcal{X}_i)$;
 // regularization when estimating of \mathbf{U}_d can be used.
- 6 **end**
- 7 $\hat{\mathcal{G}}^{(t)} = \operatorname{argmax}_{\mathcal{G}} \sum_{i=1}^n l(\mathcal{G}, \hat{\mathbf{U}}_1^{(t)}, \hat{\mathbf{U}}_2^{(t)}, \dots, \hat{\mathbf{U}}_D^{(t)} | y_i, \mathcal{X}_i)$;
 // regularization when estimating \mathcal{G} can be used.
- 8 $\hat{\mathcal{B}}^{(t)} = \hat{\mathcal{G}}^{(t)} \times_1 \hat{\mathbf{U}}_1^{(t)} \times_2 \hat{\mathbf{U}}_2^{(t)} \times_3 \dots \times_D \hat{\mathbf{U}}_D^{(t)}$;
- 9 **if** $\|\hat{\mathcal{B}}^{(t)} - \hat{\mathcal{B}}^{(t-1)}\|_1 \leq \eta$ **then**
- 10 $s = 1$;
- 11 **end**
- 12 $t \leftarrow t + 1$;
- 13 **end**
- 14 Output $\hat{\mathcal{B}}^{(t)}$.

Algorithm 3: TR based on CP decomposition (Zhou et al., 2013)

input : data (\mathcal{X}_i, y_i) for $i = 1, \dots, n$; maximum iterations T ; stopping threshold η
output: estimated coefficient tensor $\hat{\mathcal{B}}$

- 1 Initialize $\hat{\mathbf{U}}_d^{(0)} \in \mathbb{R}^{I_d \times R}$ for $d = 1, 2, \dots, D$;
- 2 $t \leftarrow 1$, convergence status $s \leftarrow 0$;
- 3 **while** $t \leq T$ and $s = 0$ **do**
- 4 $d \leftarrow 1$;
- 5 **for** $d = 1$ to D **do**
- 6 $\hat{\mathbf{U}}_d^{(t)} = \operatorname{argmax}_{\mathbf{U}_d} \sum_{i=1}^n l(\hat{\mathbf{U}}_1^{(t)}, \dots, \hat{\mathbf{U}}_{d-1}^{(t)}, \mathbf{U}_d, \hat{\mathbf{U}}_{d+1}^{(t-1)}, \dots, \hat{\mathbf{U}}_D^{(t-1)} | y_i, \mathcal{X}_i)$;
 // regularization when estimating \mathbf{U}_d can be used.
- 7 **end**
- 8 $\hat{\mathcal{B}}^{(t)} = \sum_{r=1}^R \hat{\mathbf{u}}_1^{(t),r} \circ \hat{\mathbf{u}}_2^{(t),r} \circ \dots \circ \hat{\mathbf{u}}_D^{(t),r}$ where $\hat{\mathbf{u}}_d^{(t),r}$ is r^{th} column of $\hat{\mathbf{U}}_d^{(t)}$;
- 9 **if** $\|\hat{\mathcal{B}}^{(t)} - \hat{\mathcal{B}}^{(t-1)}\|_1 \leq \eta$ **then**
- 10 $s = 1$;
- 11 **end**
- 12 $t \leftarrow t + 1$;
- 13 **end**
- 14 Output $\hat{\mathcal{B}}^{(t)}$.

We run 200 repeats in each response type case and evaluated the prediction accuracy of the estimated TR models in the testing data, the accuracy of estimated or reconstructed $\hat{\mathcal{B}}$, and the accuracy in identifying zero and non-zero elements in the core tensor after the Tucker

decomposition of $\hat{\mathcal{B}}$. When identifying zero and non-zero elements in the core tensor for TR models not based on Tucker decomposition, Tucker decomposition was applied to obtain a core tensor in each case. We then set τ_0 (the threshold for zero elements in the estimate core tensor) at 0.005, 0.05, and 0.05 for the linear, logistic, and Poisson TR, respectively.

The results are summarized in Table 4. In summary, NA_0CT^2 has the smallest mean prediction error and MSE of \mathcal{B} compared to the other regression methods in all three data types. In terms of the sparsity of the core tensor, NA_0CT^2 is the only method that can effectively promote sparsity in the core tensor. While Tucker-decomposition-based TR with the ℓ_1 regularized core tensor also promotes core tensor sparsity, it is far from enough given there are 62 0’s in the core tensor in each regression case; in addition, it runs into numerical issues during the iterative optimization (during the iterations of the block relaxation algorithm in Algorithm 2, parameters are updated “blockwise” sequentially in the GLM framework with predictors $\text{vec}(\mathcal{X})$ rescaled by the rest of the parameters. If a core tensor is ℓ_1 regularized, some of the columns in the rescaled $\text{vec}(\mathcal{X})$ contain only 0’s, resulting in a design matrix not of full rank with “redundant” features). The Bayesian regression with the spike-and-slab prior promotes sparsity in a manner conceptually similar to ℓ_0 regularization but uses probabilistic modeling to achieve sparsity without a hard penalty directly on the number of non-zero coefficients. In addition, similar to the ℓ_1 regression methods in the comparison set examined in the simulation studies, the sparsity constraint is imposed on \mathcal{B} , which may not translate to sparsity on \mathcal{G} .

4.2 Real Data Application

We applied different TR methods and compared their performances in two real datasets. The first is the FG-NET dataset that contains human face images (Fu et al., 2014) (http://yanweifu.github.io/FG_NET_data/FGNET.zip); the task is age prediction given the images and identification of face areas (image pixels) that are relevant for age prediction. The second application is the KTH dataset that contains human motion videos (Schuldt et al., 2004) (<https://www.csc.kth.se/cvap/actions/>) and we aim for classification of upper vs. lower body motions and identification of video regions that are relevant for the prediction.

NA_0CT^2 is the best in terms of both prediction accuracy and feature selection ability in the FG-NET example and in feature selection in the KTH dataset and its performance is not the best or the worst in prediction accuracy in the KTH dataset. In what follows, we describe the data, the applications, and the results in detail.

4.2.1 Facial Age Prediction

The FG-NET dataset contains 1,002 human face images (color or greyscale) from 82 individuals aged from 0 to 69 years old. Each image is labeled with the person’s age and contains 68 manually annotated points, which describe the structure of a face and are located around the eyebrows, mouth, eyes, nose, and the edge of a face. We examined the performances of different TR methods in the We run linear TR with ℓ_2 loss to predict age given an image and identify pixels that are important predictors of age.

We first pre-processed the images before the model fitting. Specifically, we transformed all

Table 4: Performance comparison among TR models in 3 simulation studies (200 repeats)

regression method	mean prediction error* (SD)	MSE# of \mathcal{B}	average number of 0 in core tensor
linear TR			
NA ₀ CT ²	0.4114 (0.0181)	0.0002	62.00
unregularized Tucker	0.4487 (0.0213)	0.0011	17.50
ℓ_1 regularized Tucker	0.4393 (0.0211)	0.0008	28.64
unregularized CP	0.4415 (0.0205)	0.0009	23.22
ℓ_2 regularized CP	0.4269 (0.0203)	0.0006	26.06
vectorized	0.4487 (0.0213)	0.0011	17.50
ℓ_1 regularized vectorized	0.4490 (0.0214)	0.0011	17.46
Bayesian spike-slab	0.4484 (0.0212)	0.0324	17.02
Poisson TR			
NA ₀ CT ²	1.5639 (0.1110)	0.0051	62.00
unregularized Tucker	1.8391 (0.1626)	0.0165	25.22
ℓ_1 regularized Tucker [§]	1.8272 (0.1625)	0.0160	25.90
unregularized CP	1.8154 (0.1593)	0.0156	27.20
ℓ_2 regularized CP	1.6196 (0.1207)	0.0074	42.52
vectorized MLE	1.8391 (0.1626)	0.0165	25.23
ℓ_1 regularized MLE	1.7307 (0.1216)	0.0136	28.35
Bayesian spike-slab	2.0233 (0.1637)	0.1793	22.38
logistic TR			
NA ₀ CT ²	28.67% (0.0246)	0.1055	62.00
unregularized Tucker	29.86% (0.0288)	0.8672	3.98
ℓ_1 regularized Tucker	30.18% (0.0357)	0.6872	16.62
unregularized CP	29.85% (0.0207)	0.7542	3.00
ℓ_2 regularized CP	29.18% (0.0259)	0.2378	13.26
vectorized	29.86% (0.0288)	0.8672	3.98
ℓ_1 regularized vectorized	33.19% (0.0089)	0.3014	7.99
Bayesian spike-slab	37.41% (0.0436)	0.6908	11.11
SVM	33.84% (0.0024)	-	-

Bold numbers represent the best performer by each metric in each TR model case.

* averaged ℓ_1 prediction error $(200n)^{-1} \sum_{j=1}^{200} \sum_{i=1}^n |\hat{y}_{ij} - y_i|$ in testing data for linear and Poisson TR, where \hat{y}_{ij} is the prediction for observation i in repeat j ; averaged misclassification rate over 200 repeats in testing data for logistic TR ($\hat{y}_{ij} = 1$ if $\hat{\text{Pr}}(y_{ij} = 1) > 0.5$, where $\hat{\text{Pr}}(y_{ij} = 1)$ is for observation i in repeat j , $\hat{y}_{ij} = 0$ otherwise.)

mean squared error $\sum_{i=1}^4 \sum_{j=1}^4 \sum_{k=1}^4 (\hat{b}_{ijk} - b_{ijk})^2 / 4^3$, where b_{ijk} is the true value of element (i, j, k) in \mathcal{B} , and \hat{b}_{ijk} is its estimate averaged over 200 repeats.

§ The ℓ_1 regularized Poisson TR model with Tucker decomposition had convergence problems. The metrics were calculated using 180 out of 200 repeats that converged.

images to grayscale and used annotated points for a piecewise affine transformation that aligned the points and corners across all images. For example, the tip of the nose is located in the same position in a 2D Cartesian coordinate (xy) after transformation in each image; the same for all other points. We then stacked all transformed images to form a 3D block along the z-axis. The pre-processing procedure is illustrated with 3 examples in Figure 1.

We trained linear TR models on the final pre-processed gray-scaled 29×29 images to predict age and to identify pixels that are important for age prediction (800 images were used as the

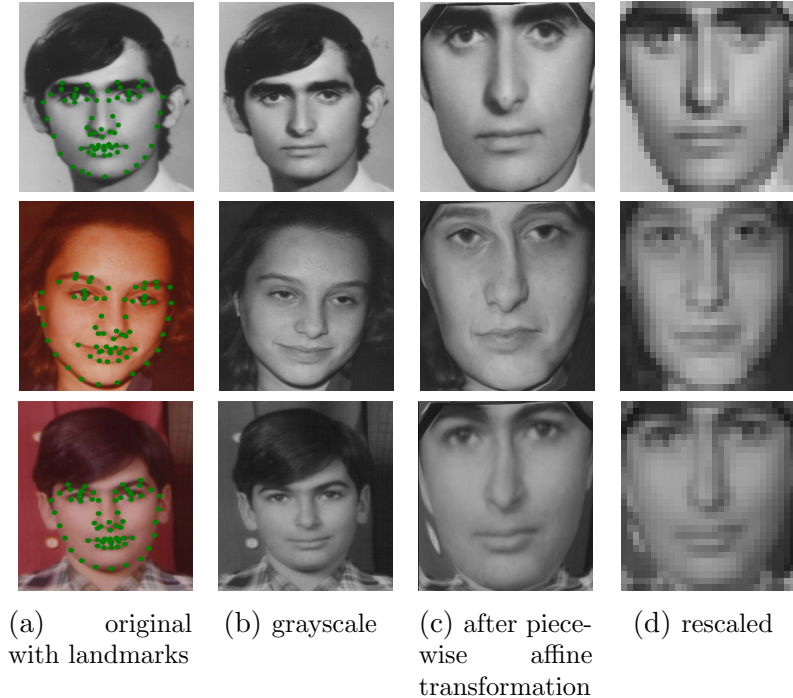


Figure 1: Pre-processing of the FG-NET images

training set, 100 images as the validation set, and the rest as the testing set).

For the NA_0CT^2 procedure, we set $n_e = 615$, $\lambda = 50$, $T = 10000$, $m = 600$, $\tau_0 = 10^{-6}$, and $\tau = 0.01$. We used the validation set to select hyperparameters n_e and core tensor dimensions R_1 and R_2 (Table 3) for NA_0CT^2 (NA_0CT^2 is relatively robust to a wide range of λ ; in the two real data examples, λ from 50 to 500 yield similar results). For other TR models that involve regularization, we merged the training and validation set and used a five-fold CV to choose the hyperparameters. For TR models without regularization, we merge the training and validation set for training.

We calculated the mean absolute prediction error $\sum_{i=1}^n |\hat{y}_i - y_i|/n$ in both real applications, where n is the number of images in the testing data, y_i is the observed response, and \hat{y}_i is predicted response from each of the fitted TR models. The results are presented in Table 5. NA_0CT^2 yields the smallest prediction error with a mean error 3.63 years, followed by the ℓ_1 regularized GLM on vectorized \mathcal{X} and \mathcal{B} , whereas the prediction errors in other TR models, regularized or not, are almost doubled or even quintupled.

Table 5: Predicted errors in different models in age prediction

NA_0CT^2	ℓ_1 regularized GLM on $\text{vec}(\mathcal{X})$	ℓ_1 -regularized Tucker	ℓ_2 -regularized CP	unregularized CP	unregularized Tucker	GLM on $\text{vec}(\mathcal{X})$
3.63	4.30	7.11	9.51	20.57	20.57	20.80

We also examined the ability of TR models on their ability to identify important pixels in age prediction based on the estimated $\hat{\mathcal{B}}$. Note that among all the TR models used, only the ℓ_1 -regularized GLM sets some of the elements in estimated $\hat{\mathcal{B}}$ at 0. Though the TR model based on the Tucker decompositions uses ℓ_1 regularization and NA_0CT^2 achieves ℓ_0 regularization,

the sparsity regularizations are imposed on the core tensor after Tucker decomposition of \mathcal{B} rather than \mathcal{B} itself, and the sparsity of the core tensor does not necessarily translate into sparsity of $\hat{\mathcal{B}}$, which is constructed from the sparse core tensor and factor matrices \mathbf{U} 's. Figure 2 depicts the histograms of the elements in estimated $\hat{\mathcal{B}}$ in each TR model. The magnitude of the elements in $\hat{\mathcal{B}}$ varies significantly across different methods. The estimated elements from NA_0CT^2 and ℓ_1 -regularized GLM are more similar in magnitude (ranging from around -1 to 1 in the former and -4 to 3 in the latter) while the other methods can produce extremely large values in $\hat{\mathcal{B}}$ (e.g, ± 70).

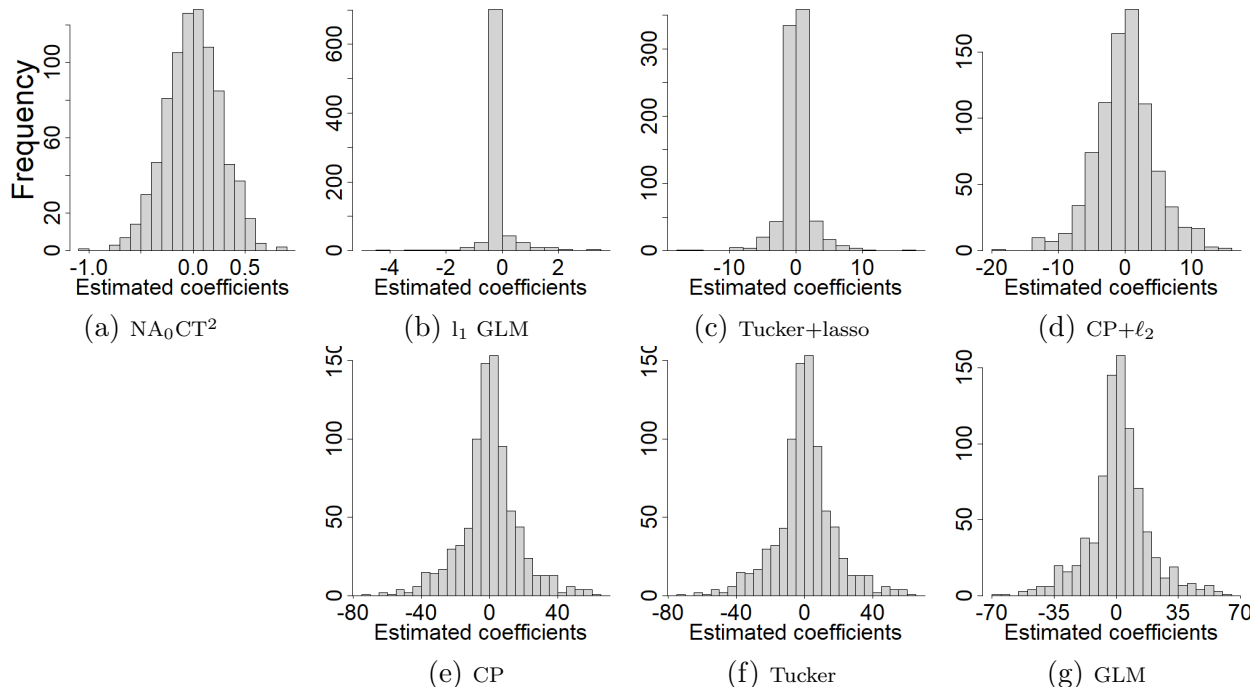
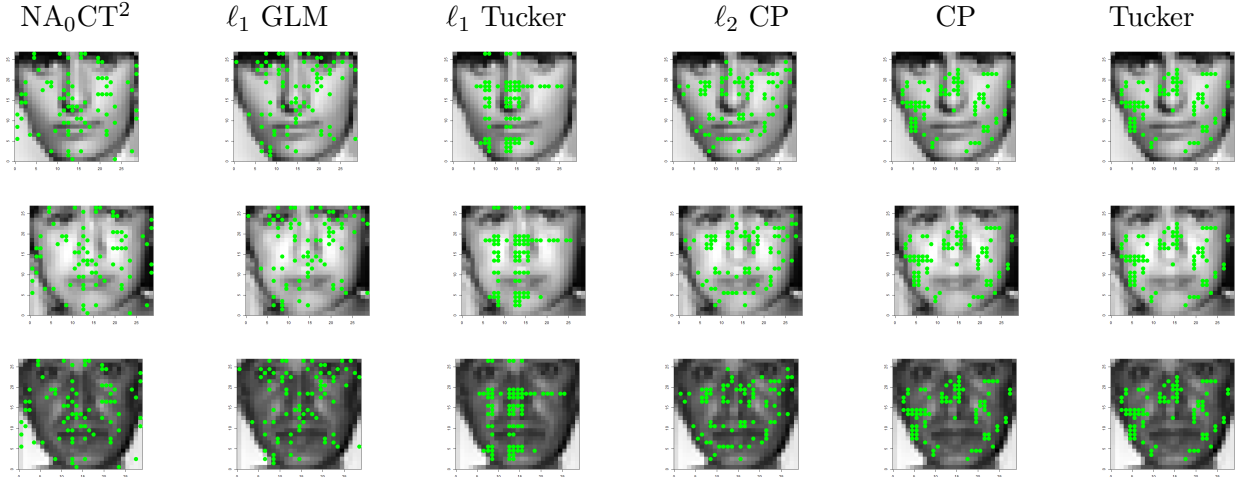
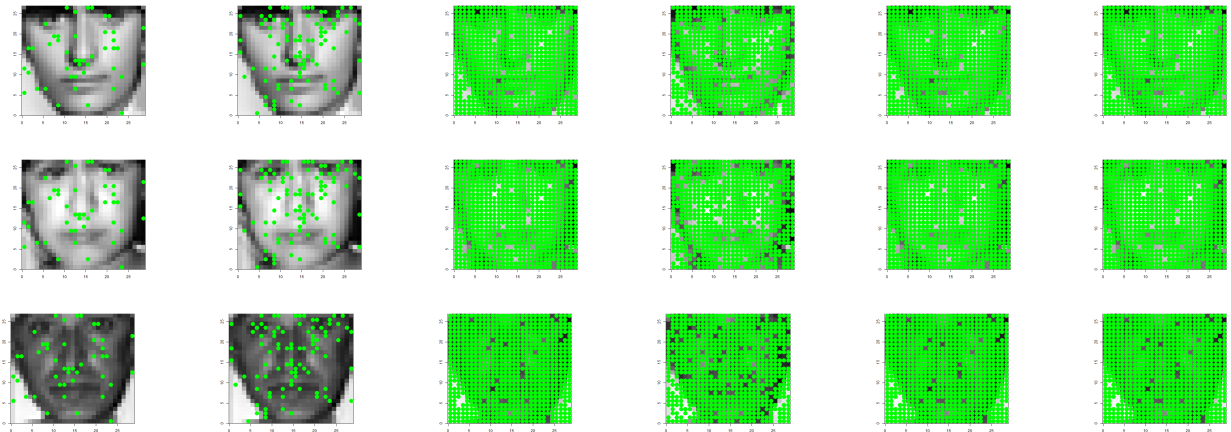


Figure 2: Histograms of estimated coefficients in different methods

We took the top 10% elements in $\hat{\mathcal{B}}$ in absolute value in each of the regression methods and plotted the corresponding pixels in Figure 3(a). We also applied hard thresholding at 0.5 to the absolute values of the elements in $\hat{\mathcal{B}}$ and plotted the pixels with corresponding elements in $|\hat{\mathcal{B}}| > 0.5$ in Figure 3(b). In both cases, the sparsity regularization imposed by NA_0CT^2 on the core tensor, though not on \mathbf{B} directly, helps to locate pixels important for age prediction, which are concentrated around eyebrows, eyes, the area under the eyes, cheekbones, laugh lines, and the area around the mouth, and jawlines, which are all related to the early signs of aging (<https://www.skinmd.ph/blog-content/2017/12/8/the-anatomy-of-an-aging-face>). The ℓ_1 regularized linear regression with vectorized predictors also identifies similar important pixels for age predictions, many of which overlap those identified by NA_0CT^2 but are more sparse. By contrast, the other TR models, regularized or not, select pixels that are not quite meaningful in terms of age prediction in Figure 3(a), or select overwhelmingly too many pixels in the hard-thresholding approach and do not help identify the important signs for age prediction.



(a) nixels corresponding to the top 10% elements in $|\hat{\mathcal{B}}|$ are plotted



(b) pixels corresponding to elements in $|\hat{\mathcal{B}}| > 0.5$ are plotted

Figure 3: Relevant pixels (green dots) for age prediction by different methods identified by two hard thresholding methods

4.2.2 Human Action Recognition

The KTH dataset contains black-white videos of 25 human subjects doing 6 different types of actions (walking, jogging, running, boxing, hand waving and hand clapping) in 4 different scenes, leading to a total of $25 \times 6 \times 4 = 600$ videos. Each video records a sequence of the same subject performing the same action in the same scene that lasts around 5 seconds and has 25 fps frame rate. Each sequence consists of a set of frames, and each frame can be viewed as a single image. Each sequences was used as one training/testing sample in our experiment. After removing sequences that don't have correct starting/ending frame stamps in a video, we ended with a total of 2259 sequences, which was split to 1697 training samples from 19 subjects and 562 testing samples from the remaining 6 subjects. For each sequence, we sampled 4 frames that were evenly distributed along the time dimension (first and last frames were always included), and rescaled each frame from the original resolution of 160×120 pixels to 4×4 . We divided each pixel value by 255 to normalize it to $[0, 1]$.

We grouped the videos types into upper body motion (1115 sequences including boxing,

hand waving and hand clapping) and lower body motion (1144 sequences including walking, jogging, running), and run logistic TR on the $4 \times 4 \times 4$ videos with negative likelihood loss to predict 2-class motion type. For the NA_0CT^2 procedure, we set $n_e = 32$, $\lambda = 50$, $T = 3000$, $m = 600$, $\tau_0 = 10^{-6}$, and $\tau = 0.01$. The core tensor in NA_0CT^2 and Tucker models (both regularized and unregularized) were of dimension $4 \times 4 \times 4$. For CP models (both regularized and unregularized), $R = 6$. The reason for choosing such dimensions is explained in Section 4 and Table 3.

We calculated the misclassification rate in each method on the motion categorization in the testing data and present the results in Table 6. We took the top 20% elements in the estimated $\hat{\mathcal{B}}$ in absolute value in each methods and plotted the corresponding pixels (green dots) in Figure 4 for two videos from a randomly selected subject. In term of classification accuracy, NA_0CT^2 's performance is in the middle, worse than ℓ_2 -regularized CP and elastic net (EN)-regularized Tucker, similar to ℓ_1 regularized GLM, and better than the 3 unregularized models. On the other hand, the image areas relevant for classification identified by NA_0CT^2 make the most sense among all the methods. Specifically, first, the selected pixels concentrated on frames 4 and 1 the most, indicating these two frames were the most important frame in terms of distinguishing the two types of motion. This is indeed the case, frames 4 and 1 have either no human or the human is located in the most right or left part of the images in videos with lower body motions. In contract, the human always shows up in videos with upper body motions. NA_0CT^2 is the only method that did not select any pixel from frames 2 and 3, indicating that its ability to focus on the most important frames. second, the middle two column pixels in each frames are also important for distinguishing the two motion types. The human is always in the middle of an image in videos containing upper body motions, and the human's position across images in the sequence in videos containing lower body motions. NA_0CT^2 selected a total of 5 pixels while the other methods picked 6 to 11 pixels from the middle two pixel columns in all frames, indicating that NA_0CT^2 can identify the most important positions in a single frame as well. Taken together, the results from NA_0CT^2 were the most interpretable.

Table 6: Motion misclassification rate by different models

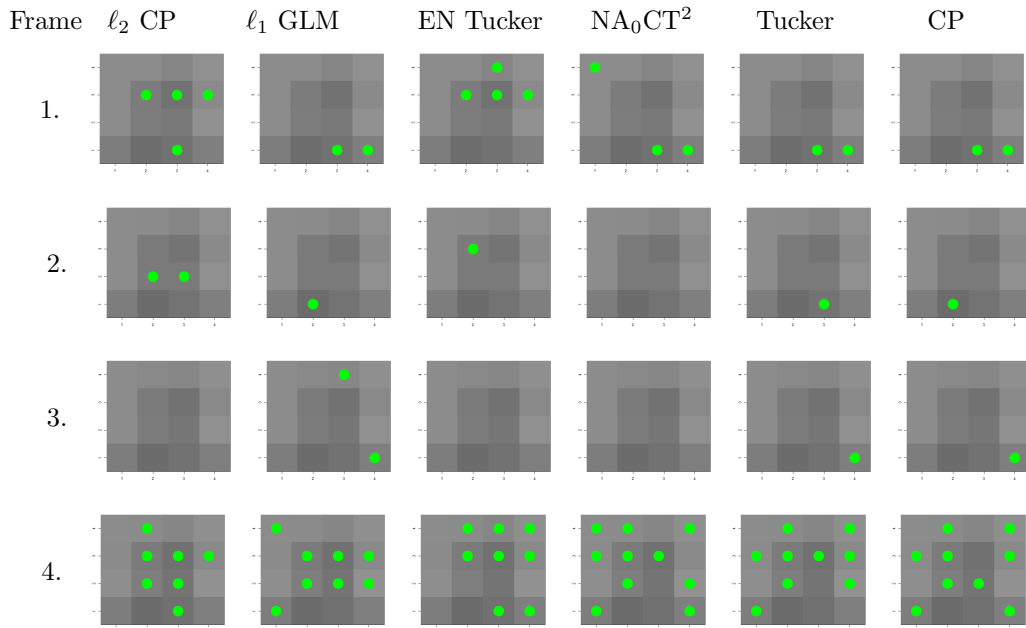
ℓ_2 -regularized CP	EN [†] -regularized Tucker	ℓ_1 regularized GLM on $\text{vec}(\mathcal{X})$	NA_0CT^2 unregularized	GLM unregularized on $\text{vec}(\mathcal{X})$	CP
1.96%	2.49%	3.20%	3.38%	4.98%	5.16%

[†] EN: elastic net

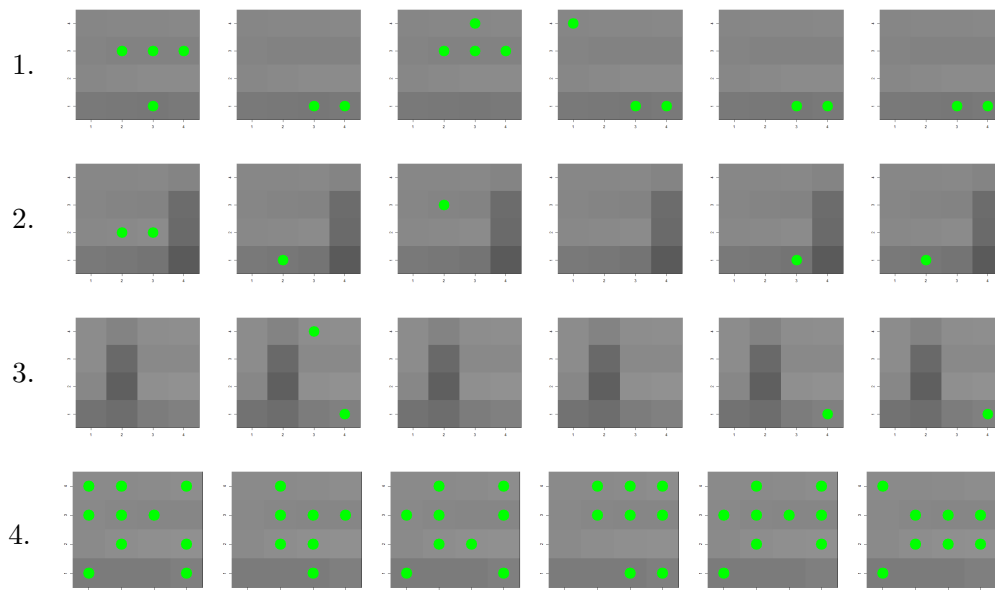
5 Discussion

We propose NA_0CT^2 , a regularization method for TR through noise augmentation, coupled with low-rank decomposition on the parameter tensor \mathcal{B} . We establish theoretically that NA_0CT^2 promotes orthogonality between the core tensor and augmented noisy data and achieves exact ℓ_0 regularization in linear and GLM TR on the core tensor in the Tucker decomposition of \mathcal{B} . To our knowledge, our method is the first Tucker decomposition-based regularization method in TR to achieve ℓ_0 in core tensors.

NA_0CT^2 is implemented through an iterative procedure. Each iteration involves two simple



(a) a processed boxing video



(b) a processed jogging video

Figure 4: Pixels (green dots) corresponding to the top 20% elements in $|\hat{\mathcal{B}}|$ estimated in each method in two example motion videos. Each row represents a single frame in videos (a) and (b), respectively. The darker vertical “post” that appears in many images represents a human subject; it does not move in each frame in video (a), reflecting that the subject stands still, doing hand motion (boxing); it moves in video (b), representing that the subject is jogging into the frame from the right and out of the frame from the left.

steps – generating noisy data based on the core tensor estimates from the Tucker decomposition of the \mathcal{B} from the last iteration and running a regular GLM on noise-augmented data with vectorized predictors. Parameter estimates from NA₀CT² are robust to the choice of hy-

perparameter λ while n_e requires careful tuning. NA_0CT^2 outperforms other decomposition-based regularization methods for TR in both simulated data and real-life data applications and can also identify important predictors though it is not designed for that purpose.

Due to the cubic time complexity in the dimensionality \mathbf{B} and \mathbf{G} in Tucker decomposition and tensor reconstruction in each iteration of the algorithm, we limited the applications of NA_0CT^2 to tensor data of relatively low dimensions in the empirical evaluations. We will continue to seek more computationally efficient approaches for Tucker decomposition and tensor re-construction so to apply NA_0CT^2 to higher-dimensional tensor datasets, such as medical imaging data, and examine its effectiveness in promoting sparsity in such settings. Since the cubic time complexity is not unique to NA_0CT^2 but also arises in other procedures involving Tucker decomposition and tensor re-construction while the noise augmentation and the GLM step in NA_0CT^2 is associated only with linear time complexity, one can be easily code and incorporate the noise augmentation step in software packages and apps that already run tensor regression with Tucker decomposition to help achieve ℓ_0 regularization for the regression.

We will also explore the asymptotic distributions of the estimated core tensor and the estimated \mathcal{B} via the NA_0CT^2 procedure, based on which confidential intervals of the parameters can be constructed. In addition, it would be of interest to quantify the convergence rate of the NA_0CT^2 procedure in n , the number of parameters in \mathcal{B} , and the number of zero elements in the core tensor, and the fluctuations around the final estimates of the estimated parameters upon convergence.

Data and Code

The data and the code for the NA_0CT^2 procedure, the simulation study, and the real data applications are available at <https://github.com/AlvaYan/NA-L0-TR>.

References

- Stephen Boyd, Neal Parikh, Eric Chu, Borja Peleato, Jonathan Eckstein, et al. Distributed optimization and statistical learning via the alternating direction method of multipliers. *Foundations and Trends® in Machine learning*, 3(1):1–122, 2011.
- J Douglas Carroll and Jih-Jie Chang. Analysis of individual differences in multidimensional scaling via an n-way generalization of “eckart-young” decomposition. *Psychometrika*, 35(3):283–319, 1970.
- Han Chen, Garvesh Raskutti, and Ming Yuan. Non-convex projected gradient descent for generalized low-rank tensor regression. *The Journal of Machine Learning Research*, 20(1): 172–208, 2019.
- Ko-shin Chen, Tingyang Xu, Guannan Liang, Qianqian Tong, Minghu Song, and Jinbo Bi. An effective tensor regression with latent sparse regularization. *Journal of Data Science*, 20(2), 2022.

- Lee Dicker, Baosheng Huang, and Xihong Lin. Variable selection and estimation with the seamless- l_0 penalty. *Statistica Sinica*, 23:929–962, 2013.
- Yanwei Fu, Timothy M. Hospedales, Tao Xiang, Yuan Yao, and Shaogang Gong. Interest-ness prediction by robust learning to rank. In *ECCV*, 2014.
- Weiwei Guo, Irene Kotsia, and Ioannis Patras. Tensor learning for regression. *IEEE Transactions on Image Processing*, 21(2):816–827, 2011.
- Richard A Harshman et al. Foundations of the parafac procedure: Models and conditions for an” explanatory” multimodal factor analysis. *Working paper*, 1970.
- Lifang He, Kun Chen, Wanwan Xu, Jiayu Zhou, and Fei Wang. Boosted sparse and low-rank tensor regression. In *Advances in Neural Information Processing Systems*, pages 1009–1018, 2018.
- Mashud Hyder and Kaushik Mahata. An approximate l_0 norm minimization algorithm for compressed sensing. In *2009 IEEE International Conference on Acoustics, Speech and Signal Processing*, pages 3365–3368. IEEE, 2009.
- Xiaoshan Li, Da Xu, Hua Zhou, and Lexin Li. Tucker tensor regression and neuroimaging analysis. *Statistics in Biosciences*, 10(3):520–545, 2018.
- Yinan Li and Fang Liu. Adaptive noisy data augmentation for regularized estimation and inference of generalized linear models. In *2022 IEEE 46th Annual Computers, Software, and Applications Conference (COMPSAC)*, pages 311–320, 2022. doi: 10.1109/COMPSAC54236.2022.00051.
- Yinan Li, Fang Liu, and Xiao Liu. Adaptive noisy data augmentation for regularized construction of undirected graphical models. In *2021 IEEE 8th International Conference on Data Science and Advanced Analytics (DSAA)*, pages 1–10. IEEE, 2021.
- Yuanyuan Liu, Fanhua Shang, Licheng Jiao, James Cheng, and Hong Cheng. Trace norm regularized candecomp/parafac decomposition with missing data. *IEEE transactions on cybernetics*, 45(11):2437–2448, 2014.
- Zhenqiu Liu and Gang Li. Efficient regularized regression with l_0 penalty for variable selection and network construction. *Computational and Mathematical Methods in Medicine*, 3456153, 2016.
- Jinchi Lv and Yingying Fan. A unified approach to model selection and sparse recovery using regularized least squares. *The Annals of Statistics*, 37(6A):3498–3528, 2009.
- Le Ou-Yang, Xiao-Fei Zhang, and Hong Yan. Sparse regularized low-rank tensor regression with applications in genomic data analysis. *Pattern Recognition*, 107:107516, 2020.
- Garvesh Raskutti, Ming Yuan, Han Chen, et al. Convex regularization for high-dimensional multiresponse tensor regression. *The Annals of Statistics*, 47(3):1554–1584, 2019.
- Samrat Roy and George Michailidis. Regularized high dimension low tubal-rank tensor regression. *Electronic Journal of Statistics*, 16(1):2683–2723, 2022.
- C. Schuldt, I. Laptev, and B. Caputo. Recognizing human actions: a local svm approach.

- In *Proceedings of the 17th International Conference on Pattern Recognition, 2004. ICPR 2004.*, volume 3, pages 32–36 Vol.3, 2004. doi: 10.1109/ICPR.2004.1334462.
- Yueyong Shi, Yuanshan Wu, Deyi Xu, and Yuling Jiao. An admm with continuation algorithm for non-convex sica-penalized regression in high dimensions. *Journal of Statistical Computation and Simulation*, 88(9):1826–1846, 2018.
- Marco Signoretto, Quoc Tran Dinh, Lieven De Lathauwer, and Johan AK Suykens. Learning with tensors: a framework based on convex optimization and spectral regularization. *Machine Learning*, 94(3):303–351, 2014.
- Xiaonan Song and Haiping Lu. Multilinear regression for embedded feature selection with application to fmri analysis. In *Thirty-First AAAI Conference on Artificial Intelligence*, 2017.
- Wei Tang, Zhenwei Shi, and Zhana Duren. Sparse hyperspectral unmixing using an approximate l0 norm. *Optik*, 125(1):31–38, 2014.
- Ledyard R Tucker. Some mathematical notes on three-mode factor analysis. *Psychometrika*, 31(3):279–311, 1966.
- Sara van de Geer. Weakly decomposable regularization penalties and structured sparsity. *Scandinavian Journal of Statistics*, 41(1):72–86, 2014.
- Ziran Wei, Jianlin Zhang, Zhiyong Xu, Yongmei Huang, Yong Liu, and Xiangsuo Fan. Gradient projection with approximate ℓ_0 norm minimization for sparse reconstruction in compressed sensing. *Sensors*, 18(10):3373, 2018.
- Kishan Wimalawarne, Ryota Tomioka, and Masashi Sugiyama. Theoretical and experimental analyses of tensor-based regression and classification. *Neural computation*, 28(4):686–715, 2016.
- Yao Lei Xu, Kriton Konstantinidis, and Danilo P Mandic. Graph-regularized tensor regression: A domain-aware framework for interpretable multi-way financial modelling. *arXiv preprint arXiv:2211.05581*, 2022.
- Hua Zhou, Lexin Li, and Hongtu Zhu. Tensor regression with applications in neuroimaging data analysis. *Journal of the American Statistical Association*, 108(502):540–552, 2013.

Appendix

A Convergence of NA_0CT^2

We examine the convergence behavior of NA_0CT^2 by presenting the trace plot of the residual deviance (the loss function in GLM) and the parameter estimates over iterations in the NA_0CT^2 algorithm in simulated studies. The data were simulated in a similar manner as in Section 4.1 except that instead of generating 8 elements which were replicated 8 times to generate \mathcal{B} , 32 elements were generated – from $\mathcal{N}(0, 1)$ in the linear and logistic cases and $\text{Unif}(0, 0.3)$ for the Poisson case – and then replicated twice to construct \mathcal{B} , leading to 32 zeros in the core tensor of \mathcal{B} . The reason for the change from the simulation settings in

Section 4.1 is that NA_0CT^2 converged very fast there with the large number of zeros (62), making it less ideal to examine the impact of m on the convergence. We decrease the number of zeros to better examine the convergence. The simulation of \mathbf{X} and Y remain the same as in Section 4.1. We set $n_e = 32$ and examined different values of m .

The trace plots of the residual deviance are presented in Figure 5 for $m = 1$ and Figure 6 for $m = 100, 300, 600$. When there is smoothing over iterations ($m = 1$) (Figure 5), the model residual deviation fluctuates significantly – due to that the noisy data used to augment the original data is a random set generated independently and differ from iteration to iteration. With the data changing from iteration to iteration, so are the parameter estimates based on the changing data, the fluctuation around the residual deviance is expected given that it is a function of both the data and parameter estimates. When $m > 1$ (Figure 6), as expected, larger m exhibits less oscillations and more stability in the loss function. $m = 600$ given much more stabilized loss function compared to $m = 1$.

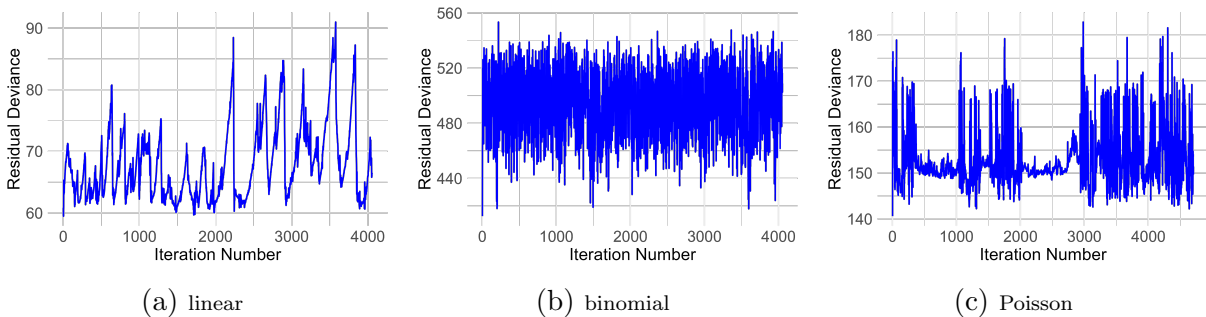


Figure 5: Example trace plot of residual deviance in a single repeated dataset in the NA_0CT^2 algorithm with $m = 1$.

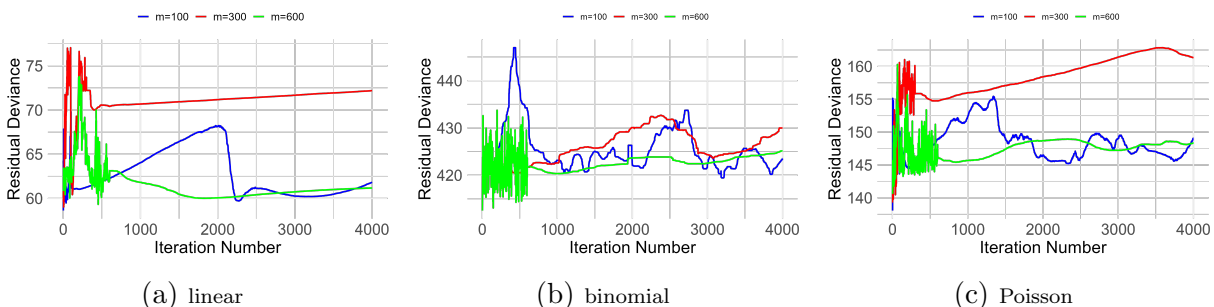


Figure 6: Example trace plot of residual deviance in a single repeated dataset in the NA_0CT^2 algorithm. The smoothing/averaging of residual deviance over m iterations does not take place until after the m -th iteration has been completed.

B Effect of n_0 on Estimated Number of Zeros in Core Tensor

In NA_0CT^2 , when the regularization parameter λ is sufficiently small but still large enough to provide effective regularization, the number of zeros in the core tensor identified by our method closely approximates the true number of zeros. As λ becomes large, the number of zeros estimated in the core tensor eventually equals the size of n_e . This insight is particularly useful for selecting appropriate values of n_e and λ .

To illustrate this behavior, we conducted an experiment in linear TR in simulated data. We generated \mathcal{B} in the same manner as in Appendix A with $n_0 = 32$ zeros in the core tensor. In NA_0CT^2 , we set n_e at 8, 24, 32, 40, 56. For each value of n_e , we ran the NA_0CT^2 algorithm 100 times with $\lambda = 0.01$ and present the average and standard deviation of the estimated number of zeros in the core tensor over the 100 repeats in Figure 7. When n_e is set at a value smaller than true number of zeros (32), the number of estimated zeros roughly equals to n_e . Once n_e exceeds the true number of zeros in the core tensor (32), the estimated number of zeros remains around $n_0 = 24$ regardless of n_e .

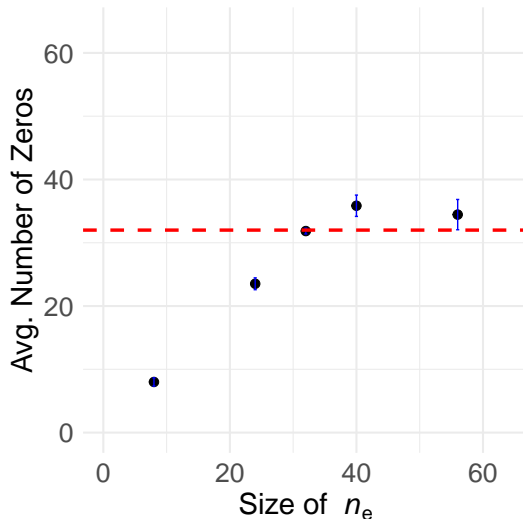


Figure 7: n_e vs. average (\pm SD) estimated number of zeros in the core tensor via NA_0CT^2 in linear TR. The dashed line represents the true number of zeros (32) in the core tensor.